

AD-783 942

**A STUDY OF THE EFFECT OF PRESSURE
GRADIENT ON THE EDDY VISCOSITY AND
MIXING LENGTH FOR INCOMPRESSIBLE
EQUILIBRIUM TURBULENT BOUNDARY LAYERS**

W. J. Glowacki, et al

**Naval Ordnance Laboratory
White Oak, Maryland**

30 May 1974

DISTRIBUTED BY:

NTIS

**National Technical Information Service
U. S. DEPARTMENT OF COMMERCE
5285 Port Royal Road, Springfield Va. 22151**

Unclassified

SECURITY CLASSIFICATION OF THIS PAGE (When Data Entered)

REPORT DOCUMENTATION PAGE		READ INSTRUCTIONS BEFORE COMPLETING FORM
1. REPORT NUMBER NOLTR 74-105	2. GOVT ACCESSION NO.	3. RECIPIENT'S CATALOG NUMBER AD 783 942
4. TITLE (and Subtitle) A Study of the Effect of Pressure Gradient on the Eddy Viscosity and Mixing Length for Incompressible Equilibrium Turbulent Boundary Layers		5. TYPE OF REPORT & PERIOD COVERED
7. AUTHOR(s) W. J. Glowacki S. W. Chi		6. PERFORMING ORG. REPORT NUMBER
9. PERFORMING ORGANIZATION NAME AND ADDRESS Naval Ordnance Laboratory Code 313, Aerophysics Division Silver Spring, Maryland 20910		8. CONTRACT OR GRANT NUMBER(s)
11. CONTROLLING OFFICE NAME AND ADDRESS		10. PROGRAM ELEMENT, PROJECT, TASK AREA & WORK UNIT NUMBERS MAT-03L-000/ZR 000-01-01
14. MONITORING AGENCY NAME & ADDRESS (if different from Controlling Office)		12. REPORT DATE 30 May 1974
		13. NUMBER OF PAGES 114
		15. SECURITY CLASS. (of this report) Unclassified
		16a. DECLASSIFICATION/DOWNGRADING SCHEDULE
16. DISTRIBUTION STATEMENT (of this Report) Approved for public release; distribution unlimited.		
17. DISTRIBUTION STATEMENT (of the abstract entered in Block 20, if different from Report)		
18. SUPPLEMENTARY NOTES		
19. KEY WORDS (Continue on reverse side if necessary and identify by block number) <div style="display: flex; justify-content: space-between;"> <div> Shear stress Turbulent Boundary layer Equilibrium </div> <div> Mixing length </div> <div> Reproduced by NATIONAL TECHNICAL INFORMATION SERVICE U S Department of Commerce Springfield VA 22151 </div> </div>		
20. ABSTRACT (Continue on reverse side if necessary and identify by block number) Shear stress, eddy viscosity, and mixing length distributions corresponding to five two-dimensional, incompressible equilibrium turbulent boundary layers were calculated by substituting measured velocity profile data into the governing equations. The five flows cover the range from moderate adverse pressure gradient to strong favorable pressure gradient.		

DD FORM 1 JAN 73 1473

EDITION OF 1 NOV 65 IS OBSOLETE
S/N 0102-014-6801

1

Unclassified

SECURITY CLASSIFICATION OF THIS PAGE (When Data Entered)

Unclassified

SECURITY CLASSIFICATION OF THIS PAGE(When Data Entered)

The calculated results show that the mixing length representation is superior for equilibrium flows and that the gradient of the mixing length in the fully turbulent region varies significantly with the pressure gradient parameter β . The observed β dependence was tested for the two adverse pressure gradient equilibrium flows. The inclusion of the β dependence affected the computed skin friction distribution significantly, greatly improving the agreement between the measured and calculated skin friction distributions.

A STUDY OF THE EFFECT OF PRESSURE GRADIENT
ON THE EDDY VISCOSITY AND MIXING LENGTH
FOR INCOMPRESSIBLE EQUILIBRIUM TURBULENT BOUNDARY LAYERS

Prepared By:

W. J. Glowacki
S. W. Chi

ABSTRACT: The purpose of this study was to improve the accuracy of turbulent boundary layer calculations by finding an expression for the turbulent shear stress which more accurately accounts for the effect of the freestream pressure gradient. Shear stress, eddy viscosity, and mixing length distributions corresponding to a number of turbulent boundary layers were calculated by substituting experimentally measured velocity profile data into the governing equations expressing conservation of mass and momentum. Distributions were obtained for five incompressible, two-dimensional boundary layers which have constant values of the pressure gradient parameter β , where β is defined as (boundary layer displacement thickness) \times (freestream pressure gradient) \div (shear stress at the wall). Such flows are referred to as equilibrium flows. The five equilibrium flows cover the range from moderate adverse pressure gradient to strong favorable pressure gradient. Where comparison is possible, the calculated distributions agree quite well with measured ones. The calculated results show that the mixing length representation is superior for equilibrium flows and that the gradient of the mixing length in the fully turbulent region varies significantly with the pressure gradient parameter β . The mixing length gradient used in current formulas does not include this pressure gradient effect and corresponds to the value obtained for zero pressure gradient (constant pressure) flows. Results for a flow in which β is changing rapidly show that the mixing length gradient lags behind that expected on the basis of the local value of β , reflecting the upstream flow history. The observed β dependence of the mixing length gradient was tested for the two adverse pressure gradient equilibrium flows using two finite-difference boundary layer computation procedures, the Cebeci-Smith procedure and one developed for this study. The inclusion of the β dependence affected the computed skin friction distribution significantly, greatly improving the agreement between the measured and calculated distributions. When used with a continuous (rather than a two-layer) mixing length formula, the observed β dependence leads to nearly perfect agreement with the experimental results.

NAVAL ORDNANCE LABORATORY
WHITE OAK, MARYLAND

NOLTR 74-105

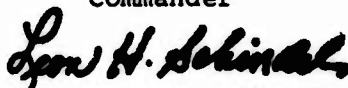
30 May 1974

A STUDY OF THE EFFECT OF PRESSURE GRADIENT ON THE EDDY VISCOSITY
AND MIXING LENGTH FOR INCOMPRESSIBLE EQUILIBRIUM TURBULENT BOUNDARY
LAYERS

This report is based on a thesis of the same title submitted by W. J. Glowacki to the Faculty of the School of Engineering and Architecture of the Catholic University of America in partial fulfillment of the requirements for the degree of Doctor of Philosophy. Professor S. W. Chi, now Associate Professor in the Department of Engineering and Applied Science, The George Washington University, Washington, D. C., was thesis advisor.

The work was supported by the Naval Ordnance Laboratory Independent Research Program under Task Number: MAT-03L-000/ZR 000-01-01, Problem 192.

ROBERT WILLIAMSON II
Captain, USN
Commander



LEON H. SCHINDEL
By direction

TABLE OF CONTENTS

CHAPTER	Page Number
1. INTRODUCTION	1
1.1 BACKGROUND	1
1.1.1 Turbulent Shear Stress and Mean-Field Methods	1
1.1.2 Eddy Viscosity and Mixing Length Concepts	4
1.1.3 Eddy Viscosity and Mixing Length Formulas	6
1.1.4 Further Improvement of Formulas	10
1.2 PURPOSE AND SCOPE OF THIS STUDY	13
2. PROCEDURES USED TO OBTAIN EDDY VISCOSITY FROM VELOCITY PROFILE DATA	16
2.1 OUTLINE OF PROCEDURE	16
2.2 DETAILS OF PROCEDURE	17
2.2.1 Data Selection.	17
2.2.2 Data Smoothing	18
2.2.3 Governing Equations and Their Solution. .	21
2.2.4 Sources of Wall Shear Stress	23
2.2.5 Freestream Velocity Gradient from Wall Shear Stress	26
3. CALCULATED SHEAR STRESS AND EDDY VISCOSITY DISTRIBUTIONS FOR SELECTED VELOCITY PROFILE DATA	30
3.1 FLOW 2400, BRADSHAW-FERRISS RELAXING FLOW ($\beta \approx 5 \rightarrow 0$)	30
3.2 FLOW 2500, BRADSHAW EQUILIBRIUM FLOW ($\beta \approx 1$)	38
3.3 FLOW 2600, BRADSHAW-FERRISS EQUILIBRIUM FLOW ($\beta \approx 5$)	40

	<u>Page Number</u>
3.4 FLOW 2700, HERRING-NORBURY EQUILIBRIUM	
FLOW ($\beta = -0.35$)	42
3.5 FLOW 2800, HERRING-NORBURY EQUILIBRIUM	
FLOW ($\beta = -0.53$)	43
3.6 FLOW 1400, WEIGHARDT ZERO PRESSURE	
GRADIENT FLOW ($\beta = 0$)	44
3.7 OVERALL VIEW OF RESULTS	46
4. TURBULENT BOUNDARY LAYER COMPUTATION PROCEDURES	
USED TO TEST EDDY VISCOSITY FORMULATION	50
4.1 CEBECI-SMITH PROCEDURE	52
4.1.1 Description of Cebeci-Smith	
Procedure	52
4.1.2 Tests of Cebeci-Smith Procedure	
for Flow 2600	54
4.2 PROCEDURE DEVELOPED FOR THIS STUDY	57
4.2.1 Description of Present Procedure	58
4.2.2 Tests of Present Procedure for	
Flow 2600	59
4.2.3 Tests of Present Procedure for	
Flow 2500	61
5. SUMMARY AND CONCLUSIONS	63
REFERENCES	67

LIST OF FIGURES

- Figure
- 1-1 Effect of Freestream Pressure Gradient on Wall Mixing Length Constant A^+
 - 3-1 Comparison of Experimental and Calculated Shear Stress Distributions for Flow 2400, Bradshaw-Ferriss Relaxing Flow ($\beta=5+0$)
 - 3-2 Comparison of Experimental and Calculated Eddy Viscosity Distributions for Flow 2400, Bradshaw-Ferriss Relaxing Flow ($\beta=5+0$)
 - 3-3 Comparison of Experimental and Calculated Mixing Length Distributions for Flow 2400, Bradshaw-Ferriss Relaxing Flow ($\beta=5+0$)
 - 3-4 Comparison of Experimental and Calculated Mixing Length Distributions in Wall Region for Flow 2400, Bradshaw-Ferriss Relaxing Flow ($\beta=5+0$)
 - 3-5 Calculated Distributions for Flow 2400, Bradshaw-Ferriss Relaxing Flow ($\beta=5+0$)
 - 3-6 Calculated Distributions for Flow 2500, Bradshaw Equilibrium Flow ($\beta=1$)
 - 3-7 Calculated Distributions for Flow 2600, Bradshaw-Ferriss Equilibrium Flow ($\beta=5$)
 - 3-8 Calculated Distributions for Flow 2700, Herring-Norbury Equilibrium Flow ($\beta=-0.35$)
 - 3-9 Calculated Distributions for Flow 2800, Herring-Norbury Equilibrium Flow ($\beta=-0.53$)
 - 3-10 Velocity Distributions in Wall Region for Flow 1400, Wieghardt-Tillmann Zero Pressure Gradient Flow ($\beta=0$)
 - 3-11 Calculated Distributions for Flow 1400, Weighardt-Tillmann Zero Pressure Gradient Flow ($\beta=0$)

Figure

- 3-12 Variation of Inner Mixing Length Constant With Pressure Gradient Parameter β for Equilibrium Flows
- 4-1 Effect of Inner Mixing Length Constant on Calculated Skin Friction Distribution Using Cebeci-Smith Procedure and Eddy Viscosity Model
- 4-2 Effect of Inner Mixing Length Constant on Calculated Skin Friction Distribution Using Cebeci-Smith Procedure
- 4-3 Effect of Inner Mixing Length Constant on Calculated Skin Friction Distribution Using Present Procedure
- 4-4 Skin Friction Distributions Calculated With Suggested Mixing Length Formula Using Various Procedures -- Flow 2600, Bradshaw-Ferriss Equilibrium Flow ($\beta=5$)
- 4-5 Skin Friction Distributions Calculated With Various Mixing Length Formulas -- Flow 2500, Bradshaw Equilibrium Flow ($\beta=1$)

LIST OF TABLES

TABLE

- 2-1 Dimensionless Wall Shear Stresses (C_f) from Various Sources
- 2-2 Freestream Velocity and Gradients Used
- 3-1 Pressure Gradient Parameter β from Various Sources

LIST OF SYMBOLS

- A^+ dimensionless wall mixing length parameter (see equation (1.12)).
- a exponent in freestream velocity distribution, $u_e \propto x^a$.
- C_f skin friction coefficient, $C_f = \frac{\tau_w}{\rho u_e^2}$
- k_1 dimensionless inner mixing length parameter (see equation (1.12)).
- k_2 dimensionless outer mixing length parameter, taken to be constant at 0.085 (see equation (4.11)).
- l mixing length, defined by $\tau_T = \rho l^2 \left| \frac{\partial u}{\partial y} \right| \frac{\partial u}{\partial y}$.
- p^+ dimensionless pressure gradient parameter, $p^+ = \frac{v}{\rho u_\tau^3} \frac{dp}{dx}$.
- p pressure (assumed equal to p_e).
- p_e freestream pressure.
- u flow velocity in x direction.
- u_e freestream flow velocity.
- u_{REF} reference freestream flow velocity for Flows 2400, 2500, and 2600, $u_{REF} = 110$ ft/sec.
- u_τ shear (or friction) velocity, $u_\tau = \sqrt{\frac{\tau_w}{\rho}}$.
- u' fluctuating component of instantaneous velocity in x direction.
- u^+ dimensionless velocity, $u^+ = \frac{u}{u_\tau}$.
- v flow velocity in y direction.
- v' fluctuating component of instantaneous velocity in y direction.
- x distance along wall in flow direction.

- y distance normal to wall and flow direction.
- y^+ dimensionless distance normal to wall, $y^+ = \frac{u_\tau y}{\nu}$.
- β dimensionless pressure gradient parameter, $\beta = \frac{\delta^*}{\tau_w} \frac{dp_e}{dx}$.
- δ boundary layer thickness, defined as y at which $u = 0.995 u_e$.
- δ^* displacement thickness, $\delta^* = \int_0^\delta (1 - \frac{u}{u_e}) dy$.
- ϵ eddy viscosity, defined by $\tau_T = \rho \epsilon \frac{\partial u}{\partial y}$.
- η dimensionless distance normal to wall, $\eta = \frac{y}{\delta}$ (except in Section 4.1.1).
- θ momentum thickness, $\theta = \int_0^\delta (1 - \frac{u}{u_e}) \frac{u}{u_e} dy$.
- μ fluid viscosity.
- ν kinematic viscosity, $\nu = \frac{\mu}{\rho}$.
- ρ fluid density.
- τ total shear stress, $\tau = \tau_L + \tau_T$.
- τ_L laminar shear stress, $\tau_L = \mu \frac{\partial u}{\partial y}$.
- τ_T turbulent shear stress.
- τ_w wall shear stress.

CHAPTER 1

INTRODUCTION

The accurate prediction of turbulent boundary layer growth is of importance for a great number of fluid-dynamic problems. In recent years, substantial improvements have been made in the numerical procedures used to calculate turbulent boundary layers. Unfortunately, these improvements have not been matched by equivalent improvements in the physics input required for the numerical calculations. As will be described in more detail below, the purpose of this study is to improve the required physics input.

1.1 BACKGROUND

1.1.1 Turbulent Shear Stress and Mean-Field Methods

The instantaneous motion of a turbulent fluid is governed by the Navier-Stokes equations which express the conservation of momentum and the continuity equation which expresses the conservation of mass for the flow. However, these equations for the instantaneous motion are extremely difficult to solve. Moreover, it is usually the mean motion of the fluid that is of interest. Therefore, equations governing the mean motion are obtained from the instantaneous equations by replacing the instantaneous value of each

variable by the sum of its mean value and its instantaneous fluctuation from the mean value, and then averaging the equations over a suitable time period. However, this procedure introduces a turbulent stress tensor, whose components are the time-averages of the products of the fluctuating velocity components and are often called the Reynolds stresses. For most two-dimensional turbulent boundary layers, the only important component is the turbulent shear stress $-\rho \overline{u'v'}$, although for some flows the normal stress component $-\rho \overline{v'^2}$ can also be important. In these expressions, ρ is the fluid density and u' and v' are the fluctuating velocity components along and normal to the flow direction.

To eliminate the need for the turbulent shear stress distribution through the boundary layer, the partial differential equations governing the mean motion of the fluid are frequently integrated in the direction normal to the flow to give an ordinary differential equation in terms of integral boundary layer parameters and the shear stress at the wall. Although such integral approaches still require additional input in the form of auxiliary equations or empirical relations, they are usually easy to solve and many have been in use for years. However, today integral methods no longer offer any real advantage over differential methods which give a more detailed description of the boundary layer and are easily adapted to many different types of flow situations. In the proceedings [1] of a conference on the computation of turbulent boundary layers held at Stanford

University in 1968, Reynolds discussed the different elements which have been used to introduce physics into turbulent boundary layer calculations, including various forms of the equations of motion, equations of state for turbulence, equations for the velocity profile and equations relating the wall shear stress to the mean flow properties. He then classified many of the calculation methods then in use according to the form of the physics input used*.

The physics input required for most differential methods of calculating two-dimensional, incompressible turbulent boundary layers is the turbulent shear stress distribution specified in the form appropriate to the particular method. As Reynolds points out, the differential methods may be divided into two groups, according to the treatment of the turbulent shear stress. The mean-field (also called mean-velocity-field) methods assume that the turbulent shear stress can be related directly to the local mean flow properties, usually the mean rate of strain. The turbulent-field methods relate the turbulent shear stress to the turbulence of the flow usually through the turbulent kinetic energy. According to the evaluation committee at the Stanford conference [1], the most successful mean-field methods were those of Cebeci and Smith [1,2] and Mellor and

*In addition, the proceedings contain fairly complete descriptions and comparative ratings of the various methods, together with a compilation of most of the good velocity profile data measured in two-dimensional, incompressible turbulent boundary layers.

Herring [1], while the most successful turbulent-field method was that of Bradshaw and Ferriss [1,3].

Although the turbulent-field methods can more properly account for the upstream turbulence history, the mean-field methods are simpler to use, require less sophisticated assumptions to specify the turbulent shear stress, and give quite good results for a wide range of flow conditions. Thus, it is most likely that the variety of different methods for specifying the turbulent shear stress now in use will continue to be used until the nature of turbulence is more fully understood and expressed in a usable mathematical form. Even then, the longer computing times that will most probably be required for the more complete treatments will necessitate the use of simpler, approximate treatments, at least, for most engineering applications. The success of mean-field methods and their intermediate position between the older integral methods and newer more detailed methods make mean-field methods a prime candidate for this role.

1.1.2 Eddy Viscosity and Mixing Length Concepts

Most mean-field methods relate the turbulent shear stress τ_T ($=-\rho\overline{u'v'}$) to the mean rate of strain $\frac{\partial u}{\partial y}$ using an eddy viscosity ϵ or a mixing length l , defined through the relations

$$\tau_T = \rho \epsilon \frac{\partial u}{\partial y} \quad (1.1)$$

$$\tau_T = \rho l^2 \left| \frac{\partial u}{\partial y} \right| \frac{\partial u}{\partial y} \quad (1.2)$$

where ρ is the fluid density, u is the mean velocity in the flow direction (along the wall), and y is the direction normal to the wall. The concept of an eddy viscosity is due to Boussinesq [4] who introduced it in analogy to the kinematic viscosity ν which relates the laminar shear stress τ_L to the same rate of strain. However, unlike the kinematic viscosity ν , the eddy viscosity is not a physical property of the fluid. It is simply a postulated proportionality constant between the turbulent shear stress and the rate of strain. On the other hand, the mixing length as introduced by Prandtl [5] has a more physical interpretation. In analogy with the mean free path used in the kinetic theory of gases, Prandtl visualized the mixing length as a mean distance transverse to the flow direction that a small mass (or lump) of fluid moves before the change in its mean velocity is equal to the mean transverse fluctuation in the flow (see Schlichting [6] for fuller details).

Schlichting considers Prandtl's mixing length to have an essential superiority over Boussinesq's eddy viscosity in that the mixing length, although still not a property of the fluid, is at least a purely local function. However, these analogies between the behavior of turbulent flow and the molecules of a gas are valid only if the "mean free path" of the turbulent eddies is small compared with the distance over

which the mean velocity gradient changes appreciably. As Bradshaw [7] points out, it is becoming more obvious that turbulent boundary layers are dominated by large eddies whose size typically is of the same order as the boundary layer thickness and that, for such large eddies, the analogies that led to the eddy viscosity and mixing length concepts are unlikely to be valid. Moreover, Champagne, Harris, and Corrsin [8] point out that even for the simplest conceivable shear flow, homogeneous turbulence maintained by a uniform mean shear, the principal axes of the turbulent stress tensor and the strain-rate tensor are not aligned, so that the defining equations for the eddy viscosity (1.1) and the mixing length (1.2) do not accurately reflect the physical situation. For boundary layers and channel flow, the misalignment is even greater. Only in the plane wake far from the symmetry axis are the principal axes of the two tensors nearly aligned.

1.1.3 Eddy Viscosity and Mixing Length Formulas

Although the validity of the eddy viscosity and mixing length concepts may be highly questionable, there is no question about the ability of eddy viscosity and mixing length formulas to predict fairly accurately the behavior of turbulent boundary layers under a wide range of flow conditions. For example, Cebeci and Smith and associates have modified and extended their combined eddy viscosity-mixing length approach, applying it to incompressible and

compressible boundary layers, with and without heat transfer and mass addition, with rather good results [1,2,9-15]. The combined eddy viscosity-mixing length approach is a result of the widespread practice of using two-layer models to represent the eddy viscosity and the mixing length distributions through the boundary layer. One formula is used in the inner (wall) region and another in the outer region with the boundary between the two regions being the point where the inner and outer formulas give the same value. From equations (1.1) and (1.2), it is seen that the eddy viscosity and the mixing length are related by

$$\epsilon = l^2 \left| \frac{\partial u}{\partial y} \right|. \quad (1.3)$$

Thus, a mixing length formula is easily used in what otherwise might be called an eddy viscosity approach.

Some of the more successful combinations used for the Stanford conference [1] are the following:

Nq-Patankar-Spalding

$$\text{inner} \quad l = 0.435 y \left[1 - \exp \left(-\frac{y}{25.3\nu} \sqrt{\frac{\tau_w}{\rho}} \right) \right] \quad (1.4)$$

$$\text{outer} \quad l = 0.09 y_{0.99} \quad (1.5)$$

Cebeci-Smith

$$\text{inner} \quad l = 0.4 y \left[1 - \exp \left(-\frac{y}{26\nu} \sqrt{\frac{\tau_w}{\rho} + \frac{dp_e}{dx} \frac{y}{\rho}} \right) \right] \quad (1.6)$$

$$\text{outer} \quad \epsilon = 0.0168 u_e \delta^* \left[1 + 5.5 \left(\frac{y}{\delta} \right)^6 \right]^{-1} \quad (1.7)$$

Mellor-Herring

$$\text{inner} \quad \epsilon = \frac{\nu \chi^4}{\chi^3 + (6.9)^3} \text{ where } \chi = 0.41 \frac{y}{\nu} \sqrt{\frac{\tau}{\rho}} \quad (1.8)$$

$$\text{outer} \quad \epsilon \approx \epsilon + \nu = 0.016 u_e \delta^* \quad (1.9)$$

In these expressions, τ is the total shear stress, τ_w is the wall shear stress, $y_{0.99}$ is the value of y at which the flow velocity u equals 99% of its freestream value u_e , p_e is the freestream pressure, and δ and δ^* are the boundary layer and displacement thicknesses, respectively.

It is seen that the inner mixing length formulas used by Ng, Patankar, and Spalding and by Cebeci and Smith are quite similar, both being slight variations of the modified form of the Prandtl mixing length

$$l = 0.4 y \left[1 - \exp \left(- \frac{y}{26\nu} \sqrt{\frac{\tau_w}{\rho}} \right) \right] \quad (1.10)$$

proposed by Van Driest [16] to account for viscous damping at the wall. Because the Van Driest formula was derived for constant freestream pressure flows, Ng, Patankar, and Spalding replace the wall shear stress τ_w by the local shear stress τ to account for non-zero freestream pressure gradients. Cebeci and Smith do essentially the same thing, but use a simple expression for τ which is a good approximation very near the wall where the Van Driest damping factor has an influence. In the outer region, Ng, Patankar, and Spalding use a constant mixing length, while Mellor and Herring use a constant eddy viscosity as first suggested by Clauser [17]. Cebeci and

Smith also use Clauser's eddy viscosity but modify it using an approximate formula for Klebanoff's intermittency factor [18] which attempts to correct for the fact that the flow in the outer region is only intermittently turbulent.

Examination of the eddy viscosity formulas shows that the influence of a freestream pressure gradient is confined to the changes it makes in the local shear stress in the inner region. Similarly, the freestream pressure gradient influences the mixing length only through the local shear stress but now only in the very thin region near the wall where the exponential term in the Van Driest damping factor is not negligibly small. The same behavior is observed in one of the few continuous mixing length formulas. Chi and Chang [19] have fitted mixing length results derived from the Coles' law of the wake [20] using zero pressure gradient data by the single formula

Chi-Chang

$$\frac{l}{\delta} = \left(0.4\eta - 0.5\eta^2 + 0.2\eta^3 \right) \left[1 - \exp\left(-\frac{Y}{20\nu} \sqrt{\frac{\tau_w}{\rho}}\right) \right] \quad (1.11)$$

$$\eta = \frac{Y}{\delta}$$

valid through the entire boundary layer. If this formula is extended to flows with pressure gradient in the same way as was Van Driest's formula given by equation (1.10), then the pressure gradient again affects the mixing length only through the local shear stress very close to the wall.

1.1.4 Further Improvement of Formulas

There now is theoretical and experimental evidence that the effect of pressure gradient on the mixing length is not confined to a change in the local shear stress. For convenience, the inner mixing length formula will be defined in terms of the general form

$$l = k_1 Y \left[1 - \exp \left(- \frac{Y}{A^+ v} \sqrt{\frac{\tau}{\rho}} \right) \right] \quad (1.12)$$

Cebeci [13] solved an approximation to the momentum equation in the viscous sublayer immediately adjacent to the wall and obtained an expression for A^+ which reduces for a non-porous wall (no mass transfer) to

$$\text{Cebeci} \quad A^+ = A_0^+ \sqrt{\frac{\tau}{\tau_w}} (1 + 11.8 P^+)^{-\frac{1}{4}} \quad (1.13)$$

where A_0^+ is the zero pressure gradient, zero mass transfer value of A^+ (Cebeci used $A_0^+ = 26$) and P^+ is defined by

$$P^+ = \frac{v}{\rho u_\tau^3} \frac{dp}{dx} \quad (1.14)$$

$$\text{with} \quad u_\tau = \sqrt{\frac{\tau_w}{\rho}} \quad (1.15)$$

(It should be noted that A^+ and P^+ are defined differently than the quantities used by Cebeci.)

At about the same time, from an examination of experimental velocity profiles measured under a wide range of flow conditions, Kays [21] obtained an expression for A^+ which reduces for a non-porous wall to

Kays

$$A^+ = A_0^+ (1 + 30.18 P^+)^{-1} \quad (1.16)$$

Although this equation was based only on accelerating flow data, Kays indicates that it may be valid for decelerating flows as well. The variation of A^+ obtained for a limited range of P^+ is shown in Figure 1-1. Kays also indicates that a rate equation for A^+ might be necessary to account for the lag observed when P^+ is changing very rapidly.

In addition to A^+ , the pressure gradient has been observed to affect the other mixing length "constant" k_1 appearing in equation (1.12). Bradshaw and Ferriss (22) measured shear stress and velocity distributions in strong adverse (positive) pressure gradient flows and calculated the corresponding eddy viscosity and mixing length distributions. Their results show values of k_1 up to about 0.6 which is considerably higher than the value of about 0.4 obtained from zero pressure gradient flow data. Although published in 1965, the results of Bradshaw and Ferriss have had little, if any, effect on current eddy viscosity and mixing length formulas.

The measurement of shear stress distributions is time-consuming, costly, and difficult for even the simplest of flows. Therefore, most "improvements" in eddy viscosity or mixing length formulas are obtained by modifying the formulas until the calculated results agree reasonably well with some experimental results. If the cause of an observed

effect can be correctly identified, then such an indirect approach has considerable merit. However, a more direct approach is available. Shear stress distributions can be extracted from measured velocity profile data using the conservation equations which govern the flow. The corresponding eddy viscosity and mixing length distributions, calculated using the defining equations (1.1) and (1.2), are free of the assumptions on form that are built into any formula. Thus, not only the values of the "constants" but also the form of the formula itself can be determined. By analyzing distributions obtained for a wide range of flow conditions, improved eddy viscosity or mixing length formulas can be obtained. In practice, however, this procedure must be carried out very carefully with good experimental data in order to obtain useful results.

This approach is not new. It has been used in different forms by a number of investigators, dating back at least to Schultz-Grunow [23] and Wiegardt and Tillmann [24], who used it to analyze their own experimental data. Escudier [25] also used this approach to obtain mixing length distributions in incompressible boundary layers, wall jets, and pipe or channel flows in an effort to determine whether the mixing length could be related uniquely to the distance from the wall. Because his results were obtained over a very wide range of flow conditions, it is very difficult to detect any definite trends. However, his results do seem to confirm the higher value of k_1 obtained by Bradshaw and Ferriss.

Spence [26], Maise and McDonald [27], Poe and Holsen [28], and Meier and Rotta [29] have applied variations of this approach to supersonic compressible boundary layers up to a Mach number of 7. Bushnell and Morris [30,31] have recently extended this range to hypersonic Mach numbers up to 20.

1.2 PURPOSE AND SCOPE OF THIS STUDY

In general, the purpose of this study is to improve the accuracy of turbulent boundary layer calculations by finding an expression for the turbulent shear stress which more accurately accounts for the effect of the freestream pressure gradient. More specifically, the purpose is to study eddy viscosity and mixing length approaches for turbulent boundary layers with freestream pressure gradients in order to determine the appropriateness of these approaches for such flows, to evaluate current formulas, and to detect possible areas of improvement. First, eddy viscosity and mixing length distributions will be extracted from existing velocity profile measurements for a number of two-dimensional, incompressible turbulent boundary layers with pressure gradients. Next, these distributions will be examined to determine the effects of the pressure gradients. Then, the most appropriate correlation of these results will be tested for boundary layers with various pressure gradients using a suitable finite-difference computation procedure.

In order to minimize effects other than those caused by the pressure gradient, this study will center on the simplest

class of two-dimensional, incompressible turbulent boundary layers with pressure gradient, the equilibrium turbulent boundary layers. The term equilibrium is used to denote a boundary layer for which the velocity profiles at various stations are similar when expressed in the non-dimensional form of $\frac{u-u_e}{u_\tau}$ versus $\frac{y}{\delta}$ (the defect form) where u_τ is the shear (or friction) velocity given by equation (1.15) and δ is the boundary layer thickness. Although exact similarity can be achieved only in a few special cases, Clauser [32] has achieved near similarity in two adverse pressure gradient boundary layers and has found [17] that for such flows the pressure gradient parameter β is constant throughout the flow. The parameter β is defined by

$$\beta = \frac{\delta^*}{\tau_w} \frac{dp_e}{dx} \quad (1.17)$$

where δ^* is the boundary layer displacement thickness, τ_w is the wall shear stress, and $\frac{dp_e}{dx}$ is the freestream pressure gradient. For incompressible flows, Townsend [33] and Mellor and Gibson [34] have shown that approximate similarity in the velocity profiles is obtained if the freestream velocity u_e varies in proportion to x^a where a is the same constant throughout the flow. Since flows with exactly similar defect profiles, flows with constant β , and flows with u_e proportional to x^a are practically indistinguishable from an experimental viewpoint, the term equilibrium is usually considered to include all three. Zero pressure gradient (constant pressure) boundary layers correspond both to $\beta=0$

and $u_e \propto x^0$ everywhere and thus are just one member of the family of equilibrium boundary layers.

The very nearly similar velocity profiles occurring in an equilibrium boundary layer indicate that the boundary layer is in a state of equilibrium under the applied free-stream pressure distribution and therefore can be considered as having a constant flow history. Because of this constant flow history, the eddy viscosity and mixing length distributions will also be in equilibrium. By comparing the distributions corresponding to different equilibrium boundary layers and therefore to different freestream pressure distributions, the effect of the pressure distribution can be determined. Although these equilibrium results may not apply directly to strongly non-equilibrium boundary layers in which the flow is far from equilibrium, the results will extend our knowledge of the eddy viscosity and mixing length from zero pressure gradient flows to flows with pressure gradient and supply a stepping-stone for a further extension to more complex flows.

CHAPTER 2

PROCEDURES USED TO OBTAIN EDDY VISCOSITY
FROM VELOCITY PROFILE DATA

2.1 OUTLINE OF PROCEDURE

The shear stress distributions for many turbulent boundary layers can be obtained by substituting measured velocity profile data into the governing equations for the conservation of mass and momentum in the flow. Appropriate data must be selected and smoothed so that the necessary derivatives along and normal to the flow direction may be evaluated with reasonable accuracy. In order to simplify the smoothing of a fairly large number of profiles, a spline-fit-with-constraints procedure was developed and programmed for computer use. The constraints are imposed to insure that the spline-fit satisfies the physical conditions at the boundaries of the flow. The spline-function and its derivative are substituted into the governing partial differential equations and the shear stress gradient normal to the wall is obtained. A fourth-order predictor-corrector integration technique is then applied to give the difference between the local shear stress and the wall shear stress as a function of distance from the wall. Choosing the wall shear stress (which can be done in a number of ways) then

gives the total shear stress distribution across the boundary layer. The turbulent shear stress, eddy viscosity, and mixing length distributions can now be calculated and plotted in suitable non-dimensional forms to help detect an appropriate correlation.

2.2 DETAILS OF PROCEDURE

2.2.1 Data Selection

At the time the search was being made for appropriate data, a copy of the data proceedings of the Stanford conference [1] became available. As these proceedings had very complete tabulations for a number of equilibrium flows, it was decided to restrict attention to the included flows, at least initially. The most well-known equilibrium flows, the two measured by Clauser, although included in the proceedings, were bypassed temporarily because of indications that these flows are rather strongly three-dimensional. Five equilibrium flows were selected for study. These included the adverse pressure gradient flow of Bradshaw and Ferriss [22] with pressure gradient parameter $\beta=5$, the adverse pressure gradient flow of Bradshaw [35] with $\beta=1$, the zero pressure gradient flow of Wieghardt [24] with $\beta=0$, and the two favorable pressure gradient flows of Herring and Norbury [36] with $\beta=-0.35$ and $\beta=-0.53$. The $\beta=-0.53$ case investigated by Herring and Norbury lies at the theoretical limit for equilibrium flows as predicted by Melior. Also included in the study was the relaxing flow of Bradshaw and Ferriss [22]

in which the flow abruptly changes from an equilibrium flow with $\beta=5$ to a zero pressure gradient flow. This last flow was included primarily as a checkout case since Bradshaw and Ferriss measured the shear stress distribution at each profile station and calculated the corresponding eddy viscosity and mixing length distributions.

2.2.2 Data Smoothing

After the selected velocity profile data was plotted and examined, it was obvious that the data would have to be smoothed at least in the y (normal to the wall) direction if the necessary derivatives were to be evaluated with reasonable accuracy. Since experimental data very near the wall either does not exist or is of questionable accuracy for the flows being studied, a search was made for a composite formula for the entire "law of the wall" region which includes the linear region at the wall and the logarithmic region somewhat further away. Generalizing the formula suggested by Spalding [37] to

$$y = Au + B \left[e^{Cu} - 1 - (Cu) - D \frac{(Cu)^2}{2} - E \frac{(Cu)^3}{6} - F \frac{(Cu)^4}{24} \dots \right] \quad (2.1)$$

a computer program was developed to evaluate the "constants" A, B, C, D, E, F by a method-of-least-squares fit to the experimental data. This program was prepared in such a way that any of the various "constants" could also be held constant at a given value or could be related to any other constant. For example, Spalding's formula corresponds to

$$A = \frac{\nu}{u_\tau^2}$$

$$B = \frac{.0118\nu}{u_\tau}$$

$$C = \frac{.4}{u_\tau}$$

$$D = E = F = 1$$

where ν is the kinematic viscosity and u_τ is the shear (or friction) velocity defined by $u_\tau^2 = \frac{\tau_w}{\rho}$. Various constant values and interrelations were used in an attempt to find one combination which would give good results for all the profiles to be used. Such a combination was not found and this procedure was set aside.

In order to smooth and differentiate the data in the outer portion of the boundary layer (outside the wall region), a spline-fit-with-constraints procedure was chosen*. The spline-function consists of a connecting set of "cubics" (third-degree polynomials) each representing one section of the data and so chosen that the values and first and second derivatives of adjacent cubics match at their connecting point (or "joint"). Given the number of cubics and the locations of the joints, the optimum fit to the experimental data is obtained by a least-squares procedure which minimizes the sum of the squares of the deviations from the data. A different choice for the number of cubics and/or the locations of the joints will result in a different fit, perhaps better or worse. The optimum locations of the joints for a given number of cubics could be found as part of the

*Full details of the spline-fit-with-constraints procedure and the associated computer program are given in Reference [38].

least-squares-fit procedure but such a procedure is very much more complicated than that encountered when the locations are specified before hand. To avoid these complications, the simpler procedure was used. The locations of the joints were varied in a cut and try manner until a satisfactory fit to the experimental data was obtained.

To ensure that the spline-fit will reproduce the observed behavior of boundary layers of the type under consideration, constraints were imposed during the fitting procedure. Since the generalized law of the wall formula given by equation (2.1) was not satisfactory, it was decided to apply the spline-fit procedure to the entire layer rather than just to the outer portion. Therefore, one constraint imposed was that the velocity at the wall be zero. At the outer edge of the boundary layer, the velocity is observed to approach the freestream velocity asymptotically. To approximate this observed behavior, the velocity was set equal to the freestream velocity at some point outside the boundary layer and at this point the velocity gradient in the normal direction was set equal to zero. The location of this point for each profile was varied until a good fit was obtained to the outermost data of that profile. These three constraints were applied for each spline-fit. For several cases, a fourth constraint was imposed to fix the velocity gradient very near the wall (the linear region), but the results were not satisfactory. Regardless of where in the supposedly linear region this fourth constraint was imposed,

the velocity gradient would not remain constant. Because this was not very satisfactory, the added refinement of the fourth constraint was not used in the data reduction.

Initially the only smoothing done was in the normal-to-the-wall direction. Since typically the number of profiles for a given flow were few and rather widely spaced, no smoothing was done in the direction along the wall. Later, in an effort to improve the quality of some results, smoothing was done on the data near the wall for two flows. The results appeared to be improved in the region near the wall where the smoothing was done. Further from the wall, the results were unchanged. This smoothing in the along-the-wall direction will be discussed later in connection with the particular flows involved (Flows 1400* and 2600).

2.2.3 Governing Equations and Their Solution

The governing equations for the flows being considered are the partial differential equations expressing the conservation of mass and momentum in steady, two-dimensional, incompressible turbulent boundary layers. For present purposes, these equations are written in the form

$$\frac{\partial v}{\partial y} = -\frac{\partial u}{\partial x} \quad (2.2)$$

$$\frac{\partial}{\partial y} \left(\frac{\tau - \tau_w}{\rho} \right) = \frac{1}{\rho} \frac{dp_e}{dx} + u \frac{\partial u}{\partial x} + v \frac{\partial u}{\partial y} \quad (2.3)$$

*These flow designations were originated by Coles and Hirst for the Stanford Conference [1], but are so convenient that they are being used in the literature.

where u, v are the velocity components in the x, y directions, respectively, ρ is the fluid density, p_e is the freestream pressure, τ represents the total shear stress, i.e., the sum of the laminar and the turbulent shear stresses, and τ_w is the value of τ at the wall. A fuller discussion of these equations and all aspects of the numerical procedures including the associated computer program is given in reference [38].

The boundary conditions at the wall are

$$v \Big|_{y=0} = 0, \quad (2.4)$$

$$\frac{\tau - \tau_w}{\rho} \Big|_{y=0} = 0. \quad (2.5)$$

Depending on which is given, the freestream pressure gradient required in equation (2.3) is obtained either from the freestream pressure distribution directly or from the freestream velocity distribution using the freestream form of equation (2.3)

$$\frac{1}{\rho} \frac{dp_e}{dx} = -u_e \frac{du_e}{dx} \quad (2.6)$$

Using the spline functions obtained by fitting the experimental velocity profile data to represent the velocity u and its derivatives, the conservation equations are

integrated numerically using a fourth-order predictor-corrector technique to obtain the normal flow velocity and the shear stress variable $\frac{\tau - \tau_w}{\rho}$ as a function of distance from the wall. The results are obtained in this form so that a number of different values can be tried for the wall shear stress τ_w without repeating the integration each time. The results are stored on tape and can now be used with any given τ_w to obtain the corresponding distributions of the shear stress and other shear dependent quantities such as the eddy viscosity and the mixing length.

2.2.4 Sources of Wall Shear Stress

In addition to the increased efficiency of the above approach, there is the advantage that, instead of requiring τ_w at the start, this method supplies a value for τ_w at the end of the integration. Since the shear stress τ approaches zero as the edge of the boundary layer is approached, the shear variable $\frac{(\tau - \tau_w)}{\rho}$ theoretically approaches a limiting value of $\frac{\tau_w}{\rho}$. Thus, a value of τ_w can be obtained from the profile data itself. This value of τ_w is susceptible to error from at least three sources; (a) any departures of the flow from two-dimensionality, (b) experimental errors in measured profile and freestream data, (c) numerical techniques used. Because of these possibilities for error, the value of τ_w as obtained from the calculations is of uncertain accuracy. Its greatest significance is probably for use in comparing with values of τ_w obtained by other means. The degree of

agreement should be the best measure of the accuracy of the results and their freedom from the errors noted above.

In addition to the method described in the previous paragraph, there are a number of methods for obtaining a value for the wall shear stress τ_w . These methods can be divided into three main categories. First, there are those methods which involve the direct measurement of τ_w at the time when the profile data is taken. Second, there are methods by which τ_w is obtained from the detailed profile data. Third, there are semi-empirical or theoretical methods for obtaining τ_w for given flow conditions from integral parameters only. In general, the best method of obtaining τ_w would be by direct measurement. However, such measurements are relatively difficult to make. For this reason, direct measurements often are not made, and when made, are of somewhat uncertain accuracy. Therefore, the value of τ_w must often be obtained by the methods of the other two categories.

Included in the second category are a number of methods for obtaining τ_w from the detailed profile data. If a sufficient number of accurately measured velocity profiles exist for the flow under study, then, as mentioned in the first paragraph of this section, integration of the partial differential equations governing the flow can be used to obtain a reasonable value for τ_w . Also included in this category

are the methods which fit a "universal" law to a single velocity profile to obtain τ_w . The logarithmic part of the "law of the wall" is most often used, but the linear part can also be used if experimental data exists close enough to the wall. The "law of the wake" can be used, as was done by Coles for the Stanford conference. The validity and accuracy of these methods depend on the "universality" of both the form of the law and the "constants" used in it. (Although the "constants" are usually considered universal, this is not a necessity. In theory, the "constants" can be chosen individually for each profile so that the best fit of the chosen form is obtained for each profile.)

In the third category are those methods which depend only on the integral parameters at each measuring station. This includes methods using semi-empirical or theoretical expressions for τ_w (usually in terms of the skin friction coefficient) such as the Ludwig-Tillmann law [39], the Spalding-Chi law [40], and others. The main difficulty with these methods is that they assume the "universality" of the law, at least for flows of a given type. Since the laws are usually obtained by fitting a limited amount of data, the assumption of "universality" is not too well proven. Also included in this category is the use of the integrated form of the governing equations known as the Von Karman momentum integral equation. This integral approach depends on the accuracy with which the necessary derivatives can be evaluated numerically or graphically and is particularly

poorly suited for flows with an adverse pressure gradient for which τ_w is obtained from a difference of two nearly equal terms.

Thus, a number of methods exist for "estimating" τ_w , each with its own advantages and disadvantages. Unfortunately, each of these methods is usually influenced by different factors, so that the various values of τ_w do not necessarily agree. However, for the flows being considered in this study, Table 2-1 shows that good agreement exists between the wall shear stresses obtained from experiment, from the Ludwig-Tillmann skin friction law, and from fits of the law of the wall or law of the wake to the profile data. Since preliminary calculations made to evaluate the accuracy of the procedure showed that the values of τ_w obtained as the residual* of $\frac{\tau - \tau_w}{\rho}$ at the edge of the boundary layer fluctuated erratically and were in extremely poor agreement with the values obtained by the other methods, the Ludwig-Tillman skin friction law was used to determine the wall shear stress τ_w in all subsequent calculations, whether or not a value had been determined experimentally.

2.2.5 Freestream Velocity Gradient from Wall Shear Stress

The value assigned to the freestream velocity gradient $\frac{du_e}{dx}$ was found to have a significant effect on the results

* This technique for obtaining τ_w will be referred to as the residual method.

obtained, particularly on the residual value of $\frac{\tau - \tau_w}{\rho}$ obtained at the outer edge of the boundary layer. However, if a realistic wall shear stress (experimental or Ludwig-Tillmann formula) is used, the effect of the freestream velocity gradient on the shear stress, eddy viscosity, and mixing length distributions is negligibly small near the wall but increases rapidly with distance through the boundary layer. A typical example of this was given in an earlier report on this work [41]. Thus the calculated shear stress distribution depends strongly on both the freestream velocity gradient and the wall shear stress used in the calculation. Thus, if both the freestream velocity gradient and the wall shear stress are chosen independently, the calculated shear stress distribution need not approach zero at the outer edge of the boundary layer, as is observed experimentally. In an effort to correct this, the freestream velocity gradient $\frac{du_e}{dx}$ which must be used to give zero shear stress at the freestream edge of the boundary layer (when the wall shear stress is obtained from the Ludwig-Tillmann skin friction law) has been determined in the following way.

The Von Karman momentum integral equation is

$$\frac{d\theta}{dx} + \left(2 + \frac{\delta^*}{\theta}\right) \frac{\theta}{u_e} \frac{du_e}{dx} = \frac{C_f}{2} = \frac{\tau_w}{\rho u_e^2} \quad (2.7)$$

with θ and δ^* being the momentum and displacement thicknesses, respectively. The derivative $\frac{d\theta}{dx}$ is difficult to determine

with the accuracy necessary to evaluate $\frac{du_e}{dx}$ from this equation as it stands. However, this difficulty can be avoided by differencing this equation for two values of $\frac{du_e}{dx}$, while noting that $\frac{d\theta}{dx}$, θ , δ^* , and u_e do not depend on the value used for $\frac{du_e}{dx}$, while $\frac{C_f}{2}$ by the residual method does. The result is

$$\left(2 + \frac{\delta^*}{\theta}\right) \frac{\theta}{u_e} \Delta\left(\frac{du_e}{dx}\right) = \Delta\left(\frac{C_f}{2}\right) \quad (2.8)$$

so that

$$\Delta\left(\frac{du_e}{dx}\right) = \frac{u_e \Delta\left(\frac{C_f}{2}\right)}{2\theta + \delta^*} \quad (2.9)$$

Thus, once a computation has been made for a particular value of $\frac{du_e}{dx}$ and the corresponding residual has been found, the above expression can be used to calculate the change in $\frac{du_e}{dx}$ necessary to make the residual have the value given by the Ludwig-Tillmann law.

This equation was used to predict the necessary changes in $\frac{du_e}{dx}$ for each of the flows. The absolute and percentage changes from the values of $\frac{du_e}{dx}$ originally used are tabulated in Table 2-2 for all the flows being considered. For most of the profiles, the changes were considered to be within the accuracy with which $\frac{du_e}{dx}$ could be obtained from the experimental freestream velocity distribution. (For flows such as 2400 and 1400 in which some of the original values

of $\frac{du_e}{dx}$ are zero or near zero, the percentage changes are rather meaningless.) Calculations were then made with the new values for $\frac{du_e}{dx}$ for each of the flows. The results will be discussed in the next chapter.

CHAPTER 3

CALCULATED SHEAR STRESS AND EDDY VISCOSITY
DISTRIBUTIONS FOR SELECTED VELOCITY PROFILE DATA

The procedure used to calculate shear stress and eddy viscosity distributions from measured velocity profile data has been presented, discussed and evaluated in Chapter 2. In this chapter, the results obtained by applying this procedure to one nonequilibrium flow and five equilibrium flows will be presented in detail. First, the results for each flow are examined and discussed individually. Then, an overall view of the results is given.

3.1 FLOW 2400, BRADSHAW - FERRISS RELAXING FLOW ($\beta=5 \rightarrow 0$)

Bradshaw and Ferriss [22] measured mean velocity, turbulent intensity, and shear stress distributions in a turbulent boundary layer which is initially in equilibrium with $\beta=5$ but is suddenly changed to a $\beta=0$ flow by the removal of the freestream pressure gradient. The measurements show that the flow is relaxing toward a typical zero pressure gradient flow but has not yet completed this relaxation by the last measuring station. For comparison, Bradshaw and Ferriss also present the distributions measured when the initial equilibrium flow is maintained in equilibrium

with $\beta=5$ throughout the measuring region. This equilibrium flow is designated as Flow 2600 and is considered in section 3.3.

As has been stated previously, this flow has been included as a test case because Bradshaw and Ferriss used a hot-wire anemometer to measure the shear stress distribution across the boundary layer at each profile station and calculated the associated eddy viscosity and mixing length distributions. Unfortunately, the freestream velocity distribution is rather uncertain for this flow. In addition to the values of the freestream velocity tabulated with each set of velocity profile data, freestream velocities at a number of other locations are presented in graphical form. (This data is tabulated in Volume II of the Stanford Proceedings [1]). A comparison shows that these two sets of freestream velocities do not agree very well. The difficulty seems to result from confusion as to whether the freestream velocity parameter tabulated with the profile data is $\frac{u_e}{u_{REF}}$ or $\left(\frac{u_e}{u_{REF}}\right)^2$. Bradshaw (see [1]) (and therefore Stanford also) chose $\left(\frac{u_e}{u_{REF}}\right)^2$. However, there is reason to believe that the tabulated quantity is $\frac{u_e}{u_{REF}}$. If the value of $\left(\frac{u_e}{u_{REF}}\right)^2$ at each profile station is obtained from a curve drawn through the tabulated freestream distribution, then the corresponding values of $\frac{u_e}{u_{REF}}$ when rounded off to two decimal places are the same as the values tabulated with the profile data. Other data plotted and tabulated by Bradshaw

support this interpretation. Consequently, some of the values of u_e used in this study are different than those tabulated by Stanford*. Since the gradient $\frac{du_e}{dx}$ is difficult to obtain with a reasonable degree of accuracy, the values of $\frac{du_e}{dx}$ used were those tabulated by Stanford*. It was recognized that these values were probably not right for the values of u_e used, but this choice represented a convenient starting point.

The shear stress distribution measured by Bradshaw is shown as Figure 3-1a. Bradshaw labels the ordinate of this figure as the turbulent shear stress $\overline{u'v'}$ non-dimensionalized by the square of a reference velocity. However, the curves do not go to zero at the wall but instead go to the value corresponding to the tabulated wall shear stress. Accordingly, it has been assumed that the plotted shear stress is the total (turbulent and laminar) shear stress rather than the turbulent shear stress alone. Only near the wall do the total and turbulent shear stresses differ appreciably. For example, near the peaks of the curves, the laminar shear stress is only one-thousandth of the turbulent shear stress.

For comparison to Bradshaw's results shown in Figure 3-1a, the total shear stress distributions calculated using the procedure described in the previous chapter with the Stanford values of $\frac{du_e}{dx}$ and the Ludwig-Tillmann law are shown

*The values of the freestream velocity and its gradient used in all results presented are tabulated in Table 2-2.

in Figure 3-1b. The orderly progression seen in Bradshaw's results where the peak of the curve moves downward and away from the wall as the flow proceeds downstream is missing in Figure 3-1b where the Stanford values of $\frac{du_e}{dx}$ are used. Moreover, the peak values are a good bit larger than those of Bradshaw and Ferriss, even though the values of the wall shear agree rather well with the experimental values (Table 2-1).

If the values of $\frac{du_e}{dx}$ are changed so that the freestream shear stresses are forced to be zero, then the calculated shear stress distributions are those shown in Figure 3-1c. The calculated distributions now have exactly the same behavior as the experimental results and the two sets of curves look very much alike. Unfortunately, the peak values are still too high, but even here the results are improved. For profiles 2403 to 2407, the peak values have moved closer to the experimental values. Only for profiles 2401 and 2402 are the results poorer in terms of the peak values. Moreover, the results for profile 2401 are less reliable and should be discounted somewhat because at the first profile station it is necessary to use the forward difference scheme to obtain $\frac{\partial u}{\partial x}$ rather than the more accurate central difference scheme.

Although a similar statement can be made for profile 2407, the calculated and experimental results for that profile are in rather good agreement. From the results shown in Figure 3-1, it appears that the agreement between calculated and experimental results is improved substantially

by using for $\frac{du_e}{dx}$ the values required to make the freestream shear stresses zero.

The calculated results for this flow give an excellent justification of the basic approach and the detailed procedure used in this study. First, it is seen that for reasonable values of $\frac{du_e}{dx}$, such as the Stanford values, the calculated behavior is qualitatively correct. For example, for profiles 2405, 2406, 2407, Figure 3-1b shows that, although the initial shear stress gradient is zero, the calculated shear stress rises above the wall value before decreasing in the outer portion of the boundary layer, matching qualitatively the experimental behavior shown in Figure 3-1a rather than the behavior normally expected for a zero pressure gradient flow. Secondly, it is seen that by using the present method (forcing the freestream shear stress to zero) for obtaining improved values of $\frac{du_e}{dx}$, the calculated shear stress distributions are in excellent qualitative and rather good quantitative agreement with the experimental results.

For this and each of the five equilibrium flows discussed in the later sections of this chapter, calculations of the shear stress, eddy viscosity, and mixing length distributions were carried out with the two sets of freestream velocity gradients given in Table 2-2. In every case, the distributions calculated with the final freestream velocity gradient (obtained by requiring the freestream shear stress to be zero at each profile station as described

in Section 2.2.7) behaved more as expected and, where comparison was possible, were in substantially better agreement with available experimental results. Consequently in the remainder of this chapter, only those results calculated using the final freestream velocity gradients will be presented.

The eddy viscosity distributions derived by Bradshaw and Ferriss from their experimental shear stress and velocity distributions are shown as Figure 3-2a. Near the wall, the eddy viscosity distributions for all profile stations tend to collapse into a single curve when plotted in the non-dimensional form of $\frac{\epsilon}{u_e \delta^*}$. In the outer portion of the boundary layer, the distributions diverge, broadening and reaching higher peak values as the flow proceeds downstream. Note that the dimensionless eddy viscosity for this flow exceeds the value of .016 used in many current eddy viscosity formulas. Figure 3-2b shows the calculated eddy viscosity distributions. Comparison to the experimental distributions of Figure 3-2a shows the results to be in excellent qualitative and reasonably good quantitative agreement.

The mixing length distributions obtained by Bradshaw and Ferriss are shown as Figure 3-3a. The mixing length is seen to increase rather linearly with distance from the wall for a distance of about 0.7 inch from the wall and then to remain relatively constant for the rest of the way through the boundary layer. The value at which the mixing length

levels out increases as we proceed downstream. For each of the seven distributions, the slope of the mixing length in the linear region is significantly greater than 0.40, a value typical of most current mixing length formulas. As might be expected from the shear stress and eddy viscosity distributions, the calculated mixing length distributions shown in Figure 3-3b agree very well with the experimental results.

With the overall mixing length distributions presented in Figure 3-3a, Bradshaw and Ferriss tabulate values of $\frac{l}{y}$ near the wall for each of the seven profiles of Flow 2400. In order to compare the tabulated values of $\frac{l}{y}$ with the calculated results, the results must be shown on a larger scale. This is done in Figure 3-4. Approximately 15 percent of the boundary layer is represented by the calculated mixing length results shown as open or filled circles. The solid lines are drawn with the slope given by Bradshaw and Ferriss. Short vertical lines near $\frac{l}{\delta} = .03$ mark the inner five percent of the boundary layer. Longer vertical lines near $\frac{l}{\delta} = .06$ indicate the ten percent marks for each profile. It is seen that in the inner five percent of the boundary layer, the calculated mixing length distributions have the slopes given by Bradshaw and Ferriss. Between five percent and ten percent of the way through the boundary layer the calculated results begin to deviate from the experimental slopes. Unfortunately, Bradshaw and Ferriss do not make clear just what they mean by "near $y = 0$ ".

However, the excellent agreement between the experimental and calculated results in the innermost five percent of the boundary layer must be considered another major justification of the overall approach and the detailed procedure being used in this study.

Bradshaw and Ferriss chose to present their distributions in terms of the absolute distance from the wall, i.e., in terms of y . However, the relative distance through the boundary layer expressed as $\frac{y}{\delta}$ is a more natural and reasonable (but not necessarily more correct) choice for presenting the calculated results. Similarly, most mixing length theories take the ratio $\frac{l}{\delta}$ to be constant in the outer portion of the boundary layer. Therefore the calculated results for each of the flows being considered will be presented in terms of non-dimensionalized distributions. The results discussed previously for Flow 2400 are presented in non-dimensionalized form in Figures 3-5. Several advantages to using the non-dimensionalized forms of the variables can be seen from these figures. First, in Figures 3-5a and 3-5b, the maxima of the shear stress distributions occur at very nearly the same value of $\frac{y}{\delta}$. Second, in Figures 3-5c and 3-5d, the eddy viscosity and mixing length distributions come much closer to combining into a single curve than previously. Third, in Figure 3-5d, the constant value attained by the mixing length in the outer portion of the boundary layer usually falls in the range from .096 to .16, as compared, for example, to the value of .096 used in many mixing length

formulas. It is difficult to know from these results if this spread in values of $\frac{\delta}{\delta^*}$ is significant or merely results from inaccuracies in the calculations. Further analysis of the results will be deferred until the calculated results have been presented for all the flows being considered.

3.2 FLOW 2500, BRADSHAW EQUILIBRIUM FLOW ($\beta \approx 1$)

Mean velocity measurements in an equilibrium turbulent boundary layer with $\beta \approx 1.0$ have been presented by Bradshaw [35]. While [35] contains the values of the freestream velocity u_e only at the four profile stations, Bradshaw supplied Stanford [1] with a tabulation giving u_e at 27 stations, beginning upstream and ending downstream of the four profile stations. As with Flow 2400, the agreement between the two distributions is not very good, making the values for $\frac{du_e}{dx}$ very uncertain.

The calculated shear stress distributions are shown in Figures 3-6a and 3-6b. Also shown on these figures is the measured shear stress distribution given by Bradshaw for profile 2504. The agreement between the calculated and measured results is seen to be excellent. The distributions for profile 2501 have been omitted because they were judged to be rather inaccurate. Two explanations can be given for this. First, the forward finite-difference scheme must be used at the first profile station. Second and probably more important, the boundary layer is growing very quickly for this flow. Between station 2501 and station 2502, δ ,

δ^* , and θ nearly double and by the last station (2504) they are nearly triple their values at station 2501. The value of $\frac{\partial u}{\partial x}$ calculated at station 2501 does not approach closely the specified value of $\frac{du_e}{dx}$ until about 2.5 boundary layer thicknesses from the wall. The corresponding shear stress distribution goes through a relatively deep minimum before rising and approaching a constant value. Although a few of the other 35 profiles studied showed a minimum in the shear stress distributions, the rise after the minimum was so small that the minimum could be used as the final value. Only for this case was the difference not negligible. For these reasons, the results for profile station 2501 have been disregarded.

Although it is difficult to pick values off the plot given by Bradshaw [35] with a high degree of accuracy, the agreement between the experimental results and the calculated distributions is excellent at least for the inner half of the boundary layer. The discrepancy in the outer half of the boundary layer may again be due to the fact that the boundary layer is growing very fast between stations. The eddy viscosity and mixing length distributions corresponding to the shear stress distributions of Figure 3-6b are given in Figures 3-6c and 3-6d, respectively. The distributions for station 2504 do not agree with the experimental results quite as well as did the shear stress distribution. In fact, where the shear stress agreed best near the wall, both the eddy viscosity and the mixing length agree with

Bradshaw's results better in the central portion of the boundary layer. The reason for this must lie in the values of $\frac{\partial u}{\partial y}$ used to calculate ϵ and l . Unfortunately, Bradshaw does not give any information on how he performed the necessary differentiation, so a comparison of the techniques used is not possible.

It should be remarked that different values of $\frac{du_e}{dx}$ necessarily lead to different values of β . The various values of β obtained for all of the profiles studied are tabulated in Table 3-1. The table shows that, for any of the sets of $\frac{du_e}{dx}$, β is not very constant. However, the variations in β in the table are probably small enough that the flow may still be considered an equilibrium flow with a β of about 0.9 to 1.0.

3.3 FLOW 2600, BRADSHAW - FERRISS EQUILIBRIUM FLOW ($\beta \approx 5$)

This flow is the equilibrium companion flow for the relaxing flow designated as Flow 2400. Bradshaw and Ferriss [22] state that the freestream velocity distributions are identical down to the 47-inch station. Downstream of this point, Flow 2600 remains an equilibrium flow, while Flow 2400 is rapidly changed into a constant pressure flow. As with both of the previously discussed flows (2400 and 2500), two freestream velocity distributions are given. The values used for u_e in these calculations are those tabulated for the four profile stations.

The calculated shear stress distributions are shown in Figures 3-7a and 3-7b. Again, results read from a plot given by Bradshaw [35] are shown. The agreement is not as good as for Flow 2500, although it is reasonably good in the wall region. The most probable explanation for the rather poor agreement in the outer region is the extremely rapid growth of the boundary layer between profile stations. Between the first and last stations, the boundary layer thickness has more than tripled. The relatively wide spacing between stations causes great uncertainty in the values of $\frac{\partial u}{\partial x}$. It is for this reason that the results for profile 2601 have been omitted.

The calculated eddy viscosity distributions are shown with Bradshaw's results for profile 2604 in Figure 3-7c. Again, the calculated and experimental results for profile 2604 agree reasonably well in the wall region but not so well further from the wall, reflecting the agreement in the shear stress distributions. Figure 3-7d shows that the calculated mixing length distribution is in excellent agreement with the experimental results. This agreement may be largely fortuitous since the agreement is not as good in the shear stress distributions. As was the case with the two previous flows, the mixing length distributions tend to collapse into a single curve, especially in the wall region.

Some of the velocity data near the wall looked as though it needed to be smoothed in the x direction. Since the flow changes rather drastically between the widely

spaced profile stations, simple cross-plots of u versus x and y would not help. Therefore, the four profiles were plotted in law of the wall coordinates (y^+ , u^+) and a single curve was faired through the data as far as possible. Values of u^+ versus y^+ were obtained from this curve and translated back to $\frac{u}{u_e}$ versus y to replace the unsmoothed experimental data. The differences were not very large so, when the calculations were rerun, the new distributions (shown in Figures 3-7) were virtually identical to the initial ones.

3.4 FLOW 2700, HERRING - NORBURY EQUILIBRIUM FLOW ($\beta = -0.35$)

This flow represents an equilibrium boundary layer in a mild negative pressure gradient. Neither the wall shear stress nor the shear stress distribution through the boundary layer were measured. Instead, Herring and Norbury [36] used the theory of Mellor and Gibson [34] to calculate these quantities. Since the calculated shear stress distribution could not be read with sufficient accuracy from the small figures of the original paper and since the distribution has not been recalculated using the Mellor-Gibson theory, no comparison is made between the Herring-Norbury results and those of this study.

The calculated shear stress distributions are shown in Figures 3-8a and 3-8b. The results are somewhat difficult to analyze since there are no experimental distributions with which to compare them. The distributions do show the behavior expected for a negative (favorable) freestream

pressure gradient, decreasing continuously from the wall value toward the outer edge of the boundary layer. The eddy viscosity and mixing length distributions obtained from the shear distributions of Figure 3-8b are shown in Figures 3-8c and 3-8d.

3.5 FLOW 2800, HERRING - NORBURY EQUILIBRIUM FLOW ($\beta = -0.53$)

This flow studied by Herring and Norbury [36] represents an equilibrium boundary layer in a strong negative pressure gradient. It was chosen since $\beta = -0.53$ corresponds to the limit of equilibrium flows in a negative pressure gradient, according to the theory of Mellor and Gibson [34]. As with Flow 2700, no wall shear stresses or shear stress distributions through the boundary layer were measured. Since the distribution calculated from the Mellor-Gibson theory can not be read from the published figures with sufficient accuracy, no comparison is made between the published results and those calculated here. The calculated shear stress distributions are shown in Figures 3-9a and 3-9b.

The eddy viscosity and mixing length distributions are shown in Figures 3-9c and 3-9d, respectively. However, it seems that in the inner third or so of the boundary layer, the derivative $\frac{\partial u}{\partial y}$ needs smoothing. A similar behavior was initially obtained for Flow 2700. By refitting spline-functions to the velocity profile data while taking more care to obtain a smoother derivative, the wiggles which were worse than for this flow were almost completely removed.

The resulting distributions were nearly identical to mean curves drawn through the original distributions. Because of this and the observation that the most significant findings of this study concern the results in the region near the wall where the effect of smoothing would be the least, the effort was not expended to refit the data and obtain a smoother derivative.

3.6 FLOW 1400, WIEGHARDT ZERO PRESSURE GRADIENT FLOW ($\beta=0$)

Although zero pressure gradient flows have been studied extensively, this rather classical flow was included in this study to fill in the results for $\beta=0$ and to serve as another check on the calculations. Wieghardt [24] had taken profile data at a large number of stations (23), but the amount of data at each station was very small, especially for the early profiles. For this reason, only the last ten stations were included in this study. Even then, the amount of data for each profile was rather minimal, with none of the data being taken near enough to the wall to define the profile shape near the wall.

Initially, calculations were made without smoothing in the x direction. The calculated shear stress distributions showed a very erratic behavior near the wall. When the profile data was plotted versus x rather than y , it was obvious that smoothing should be done in the x direction. Figure 3-10 shows the experimental data and curves faired through the data. Corrected values were read from the

curves. The resulting shear stress distributions shown in Figures 3-11a and 3-11b were greatly improved near the wall. The distributions were compared to the calculated distributions given by Wieghardt and the agreement was quite good.

Similar results were found for the eddy viscosity distributions where the unsmoothed (in the x direction) data produced a rather disorderly distribution. When the data was smoothed in the x direction, Figure 3-11c shows that the resulting eddy viscosity distributions tend to fall together quite well. The maximum values of the eddy viscosity curves fall reasonably close to the value of 0.016 currently being used in most eddy viscosity formulas.

Figure 3-11d shows the mixing length distributions calculated using the smoothed data. As for the eddy viscosity results, the mixing length distributions look nearly identical except for the last station 1423. On the average, the distributions level out at a value of $\frac{l}{\delta}$ of about 0.085. This value is a little lower than the value of 0.09 commonly used in mixing length formulas.

Overall, the calculated distributions appear very well behaved and in very good agreement with previous results obtained from this flow and other zero pressure gradient flows. The success of the procedure for this flow is a further justification for its use.

3.7 OVERALL VIEW OF RESULTS

In previous sections, the focus was given to each flow individually. The peculiar characteristics of the results for each flow were noted and discussed briefly, and the results were compared to experimental results wherever possible. In this section, an attempt will be made to detect and discuss the main similarities, differences, and trends present in the results as a whole.

Despite some exceptions by individual profiles, the overall results exhibit the type of behavior that was expected from previous efforts to measure or derive the distributions of shear stress, eddy viscosity, or mixing length through two-dimensional, incompressible, turbulent boundary layers. The shear stress distributions calculated in this study for positive (adverse) pressure gradients rise from the wall values, reach a maximum, then fall, reaching zero near the outer edge of the boundary layer. For zero and negative (favorable) pressure gradients, the shear stress distributions fall continuously from the wall values, also reaching zero at the outer edge of the boundary layer.

For all types of pressure gradients, the eddy viscosity rises sharply from a zero value at the wall to a maximum value of about $0.016 u_e \delta^*$ before again falling off toward zero near the outer edge of the boundary layer. The failure of many of the calculated eddy viscosity distributions to reach zero is due to the difficulty of keeping an accurate

value of the ratio of τ_T to $\frac{\partial u}{\partial y}$ as both approach zero. However, it has been found that boundary layer calculations based on an eddy viscosity concept are rather insensitive to the value of the eddy viscosity in the outer portion of the boundary layer.

Again for all types of pressure gradient, the mixing length grows nearly linearly in the wall region, then rapidly levels out to a relatively constant value of about 0.09 δ for most of the boundary layer. The values of 0.016 $u_e \delta^*$ and 0.09 δ are widely used in current eddy viscosity and mixing length theories. The variations in the calculated results about these values may or may not be a significant result of this study. It is in this outer region that the results are most sensitive to the numerical techniques, to the values used for the freestream velocity gradient, and possibly to other factors, making the validity of the calculated results more uncertain. Consequently, with the flows being considered, the significance of these observed variations cannot be determined with the desired accuracy.

On the other hand, both the eddy viscosity and the mixing length distributions for each flow tend to fall together near the wall. Actually, the mixing length distributions collapse together more than the corresponding eddy viscosity distributions do, not only in the wall region but in the outer region also. The mixing length distributions were also found to be less affected by the finite-difference scheme used to obtain $\frac{\partial u}{\partial x}$ and by the freestream velocity

gradient. Thus, the mixing length representation seems better suited to correlate the shear stress distributions in equilibrium turbulent boundary layers. The form of the mixing length distribution is similar to the ramp-type (or two-layer) model currently in use in most mixing length formulas.

The important difference shown in the present results is the departure of the slope of the mixing length in the region near the wall from the value of about 0.4 used in current formulas. A close inspection of the mixing length figures for the equilibrium flows shows definite relationship between the slope of the linear portion of the mixing length distribution near the wall and the value of the equilibrium pressure gradient parameter β . The slope k_1 decreases with decreasing β . In order of decreasing β , the equilibrium flow figures are Figures 3-7d, 3-6d, 3-11d, 3-8d, and 3-9d. The slope of the mixing length for each of the equilibrium flows is shown in Figure 3-12 as a function of β . For $\beta > 0$, these results can be fitted approximately by the formula

$$k_1 = 0.4 + 0.182257 [1 - \exp(-0.32068 \beta)] \quad (3.1)$$

As indicated by the horizontal lines on the figure, this effect of pressure gradient is not taken into account in current mixing length formulas. It should be noted that the large departure of the slope from currently used values calculated for Flow 2600 is verified by the experimental

measurements of Bradshaw and Ferriss and is supported by the calculated and experimental results for the companion relaxing flow, Flow 2400.

CHAPTER 4

TURBULENT BOUNDARY LAYER COMPUTATION PROCEDURES
USED TO TEST EDDY VISCOSITY FORMULATION

In Chapter 2, a procedure was presented for extracting shear stress, eddy viscosity, and mixing length distributions from experimental velocity profile data measured in two-dimensional, incompressible turbulent boundary layers. The results obtained for five equilibrium and one non-equilibrium flows were presented in Chapter 3. These results showed that for equilibrium flows the mixing length formulation is superior to the most widely used eddy viscosity formulation and also that the "constant" in the mixing length formula which governs the behavior in the fully turbulent region near the wall depends on the pressure gradient parameter β .

In order to test the effect of the observed variation in this "constant" due to pressure gradients, calculations were made with two turbulent boundary layer computation procedures using the mixing length formulation. Two different procedures, one taken from the literature and one developed specifically for this study, were used in an attempt to isolate the results from possible effects due to

the numerical solution techniques being used. In this chapter, the two computation procedures and the results obtained are presented and discussed.

Because it is extremely unlikely that any computation procedure will accurately predict every aspect of a boundary layer under the very wide range of conditions of practical interest, it is usually necessary to evaluate various procedures on the basis of their ability to predict a very limited number of characteristics. For example, the procedures presented at the Stanford conference [1] were evaluated primarily in terms of their ability to predict the skin friction coefficient, the Reynolds number based on the boundary layer momentum thickness, and the shape factor (the ratio of the boundary layer displacement and momentum thickness). For the present study, the effect of variations in the mixing length constants will be examined in terms of only one parameter, the skin friction coefficient. The skin friction coefficient has been chosen for a number of reasons. First, the skin friction coefficient is one of the most significant parameters in the practical application of turbulent boundary layer theory. Second, the results presented in the Stanford conference proceedings show that, for almost all of the flows included, the skin friction distributions are more uncertain and agree less well with the experimental results than either the Reynolds number or the shape factor. Third, the ability to predict the skin friction coefficient from the slope of the velocity profile

at the wall without recourse to empirical skin friction laws is one of the major advantages of the eddy viscosity and mixing length approaches over most other boundary layer computation procedures.

4.1 CEBECI-SMITH PROCEDURE

The primary purpose of the conference at Stanford [1] was to evaluate the various methods of predicting turbulent boundary layers. Twenty-seven different prediction methods were used to calculate sixteen mandatory, and up to seventeen optional, two-dimensional, incompressible turbulent boundary layers measured experimentally for a wide range of flow conditions. In addition to the detailed results for each calculation, an evaluation of the comparative success of the various prediction methods was presented. One of the methods judged most successful was that of Cebeci and Smith. Because of this and the ease with which it could be converted to an all mixing length approach, the Cebeci-Smith procedure was selected for use in this study.

4.1.1 Description of Cebeci-Smith Procedure

The finite-difference procedure used by Cebeci and Smith to solve the two-dimensional, incompressible turbulent boundary layer equations is presented briefly in [1] and in detail in [2]. The procedure as given is based on a two-layer eddy viscosity model. The boundary layer equations are first transformed to a coordinate system that removes

the singularity at $x = 0$ and stretches the coordinate normal to the flow direction. The transformations used are

$$x = x \quad (4.1)$$

$$d\eta = \left(\frac{u_e}{\nu x} \right)^{1/2} dy \quad (4.2)$$

$$\psi(x, y) = (\nu x u_e)^{1/2} f(x, \eta) \quad (4.3)$$

where
$$f' = \frac{u}{u_e}. \quad (4.4)$$

(see Symbols for definitions, if necessary). After a translated stream function defined by

$$\phi = f - \eta \quad (4.5)$$

is introduced, the streamwise derivatives are replaced by three-point finite-difference formulas.

The resulting ordinary nonlinear differential equation in ϕ is linearized, converted to finite-difference form, and solved iteratively using values from the previous iteration for those terms which had made the differential equation nonlinear. The finite-difference formulas used are derived from the Lagrange interpolation formulas and have a variable grid in the η -direction, permitting shorter steps close to the wall and longer steps away from the wall. In order to overcome oscillations and obtain convergence in the iteration process, it was necessary to use an averaging scheme on the coefficients of the finite-difference equation (2-point mean in the x -direction) and on the eddy viscosity expression (5-point mean in the η -direction).

Cebeci and Smith [2] present in detail results of tests made to evaluate the numerical techniques used as well as comparisons between calculated and experimental results for both laminar and turbulent boundary layers. Their procedure is both accurate and fast and can give quite satisfactory results for many boundary layer calculations despite the use of an eddy viscosity formulation which is based on flat-plate data. This basic method for two-dimensional, incompressible boundary layers has also been extended to compressible boundary layers, with and without heat transfer and mass addition, with rather good results.

4.1.2 Tests of Cebeci-Smith Procedure for Flow 2600

In addition to card decks for the computer program, Cebeci furnished copies of the data decks used to calculate the equilibrium boundary layer results for the conference at Stanford. Since the mixing length distributions for Flow 2600, the $\beta=5$ equilibrium flow of Bradshaw and Ferriss, give the greatest departure from current mixing length formulas for the equilibrium flows considered in this study, Flow 2600 was used as a test case for evaluating the effect of variations in the mixing length constants. The Cebeci-Smith program and Flow 2600 data were run unchanged both to check out the use of the program and to provide a baseline to which other calculations could be compared.

As was shown in equation (1.6), Cebeci and Smith express the eddy viscosity in the inner (wall) region in terms of the mixing length with a value of 0.4 for the inner constant k_1 . Before any other changes were made to the program or to the data furnished by Cebeci, a calculation was made in which the inner constant was changed from 0.4 to 0.6, the value suggested by Bradshaw's results (Figure 3-3a). Comparison of the results obtained with the values 0.4 and 0.6 indicated that the effect on the momentum thickness Reynolds number ($\sim 3\%$) and the shape factor ($< 1\%$) was negligibly small, whereas the skin friction coefficient was nearly doubled as is shown in Figure 4-1. It is seen that, for the two values used, the skin friction coefficient changes very rapidly and in opposite directions in the neighborhood of the initial station. The two distributions soon level out and become very similar, but the overall difference in level created near the initial station persists. Similar results were obtained when the eddy viscosity expression used by Cebeci and Smith in the outer region was replaced with a constant mixing length equal to 0.085δ (where δ is the boundary layer thickness). These results show that changes in the inner mixing length constant can significantly affect the calculated skin friction distribution.

Calculations incorporating the effect of pressure gradient on the inner mixing length constant k_1 were then made. The initial velocity profile given by Cebeci and Smith

was retained, but the freestream velocity distribution and its derivative were obtained from the analytical expression

$$u_e = 136.51 \left(\frac{x}{1.917} \right)^{-0.255} \quad (4.6)$$

which gives a good fit to the Bradshaw-Ferriss velocity data.

For a constant outer mixing length equal to 0.0856, calculations were made first for the Cebeci-Smith inner mixing length as given by equation (1.6), then with the constant 0.4 replaced by 0.55 as obtained from Figure 3-3b for this flow, and finally, with the constant 0.4 replaced by $k_1(\delta)$ as given by equation (3.1). The resulting skin friction distributions are presented in Figure 4-2.

This type of two-layer mixing length model results in a sharp "knee" at the junction of the inner and outer regions and, thus, overpredicts the mixing length near this junction. A continuous mixing length distribution which eliminates this "knee" and yet has the correct asymptotic behavior can be represented by

$$l = 0.0856 \tanh \left(\frac{k_1}{0.085} \frac{y}{\delta} \right) \left[1 - \exp \left(-\frac{y}{A} \right) \right] \quad (4.7)$$

where A is chosen to be

$$A = 26v \left(\sqrt{\frac{\tau_w}{\rho} + \frac{dp_e}{dx} \frac{y}{\rho}} \right)^{-1} \quad (4.8)$$

to be consistent with equation (1.6). The skin friction distribution calculated using this expression is also presented in Figure 4-2 and is seen to be in excellent agreement with the experimentally determined values.

In Chapter 3, it was shown that at least one of the constants (the inner constant k_1) appearing in current mixing length formulas varies with the freestream pressure gradient. In this section, the effect of this variation on the calculated skin friction distribution for an equilibrium turbulent boundary layer in a moderate adverse pressure gradient has been evaluated using the highly successful Cebeci-Smith computation procedure. The results showed that the calculated skin friction distribution is significantly affected by the increase in the inner constant observed in the mixing length distributions for this $\beta=5$ flow (Figures 3-3b and 3-12). The effect of possible variations in the other two mixing length constants has been found to be much less significant. To verify the results presented in this section, similar numerical experiments were made with a second computation procedure.

4.2 PROCEDURE DEVELOPED FOR THIS STUDY

The second turbulent boundary layer computation procedure used to evaluate the effect of pressure gradient on the mixing length formula constants was developed specifically for this study. As was mentioned previously, two different procedures were used in order to isolate the effect of the numerical solution techniques being used. Because the Cebeci-Smith procedure is rather elaborate and sophisticated, a very simple and straightforward procedure was chosen as the second approach to be used.

4.2.1 Description of Present Procedure

The computation procedure developed in this study, like the Cebeci-Smith procedure described earlier, approximates the governing boundary layer equations expressed in terms of an eddy viscosity by linearized, implicit finite-difference equations which must be solved iteratively. Instead of the transformations used in the Cebeci-Smith procedure, the equations are solved in the x,y coordinate system with the only transformations being from the velocity variables u and v to the dimensionless velocity ratios $\frac{u}{u_e}$ and $\frac{v}{u_e}$. Although such a simple approach may not be adequate for calculations under a wide range of flow conditions, it has proven quite adequate for the calculations made in this study.*

The nonlinear partial differential equations are solved by an iterative procedure somewhat similar to that used by Cebeci and Smith. First, the equations are linearized by assuming that the coefficients which had made the equations nonlinear are known from a previous iteration. Since these coefficients actually depend on the solution, the linearized equations must be solved repeatedly until the results of two successive iterations converge to the desired degree. The

*The basic mathematical procedure has also been used by Chi and Glowacki [42] to calculate turbulent boundary layers beneath intense vortices with very good results.

linearized differential equations are now written in the finite-difference form valid at the middle of a six-point grid (three points in y direction at two adjacent x stations). If the values of $\frac{u}{u_e}$ are known for all grid-points at the upstream station, then, using the known boundary conditions at the wall and at the outer edge of the boundary layer, the finite-difference equations can be solved for values of $\frac{u}{u_e}$ and $\frac{v}{u_e}$ for all grid-points at the downstream station. Thus, given the velocity distribution at some initial station, the calculation marches downstream, station by station, until the desired termination point is reached.

Complete details of the mathematical procedure and of the FORTRAN IV computer program using it are presented in Reference [38].

4.2.2 Tests of Present Procedure for Flow 2600

Numerical experiments, similar to those described for the Cebeci-Smith procedure, were carried out for Flow 2600 to evaluate the effect of the pressure gradient dependence of the mixing length constants on the calculated skin friction distributions. As indicated before, Flow 2600, the $\beta=5$ equilibrium flow of Bradshaw and Ferriss [22], was selected as the test case because the mixing length distributions for this flow (Figures 3-3b and 3-12) show the greatest departure from currently used formulas.

The first mixing length constant varied was the inner constant k_1 . In addition to the values of 0.4 and 0.55 used with the Cebeci-Smith procedure, calculations were made with k_1 as a function of the pressure gradient parameter β as given by equation (3.1). The calculated skin friction distributions shown in Figure 4-3 exhibit the same behavior observed in the Cebeci-Smith results of Figure 4-2. The widely used value of 0.4 underpredicts the skin friction substantially, while the "improved" value of 0.55 or the variable k_1 obtained from equation (3.1) overpredicts the experimental results. The variable k_1 distribution departs from the distribution obtained using 0.55 (corresponding to $k_1(\beta)$ when β equals the experimental value of 5.4) because the overprediction in the skin friction causes the calculated value of β to be less than 5.4. The procedure is somewhat self-correcting since a smaller value of β leads to a smaller skin friction coefficient. The skin friction distribution calculated using the continuous mixing length formula as given by equation (4.7) again is in extremely good agreement with the experimental results.

Next, pressure gradient effects on the wall mixing length parameter A occurring in the damping factor of equation (4.7) were investigated. In addition to the expression for A given by equation (4.8), the expressions

$$A = 26\nu \left(\sqrt{\frac{\tau_w}{\rho}} \right)^{-1} \quad (4.9)$$

and

$$A = 26v \left(\sqrt{\frac{\tau_w}{\rho}} \right)^{-1} (1+11.8P^+)^{-\frac{1}{2}} \quad (4.10)$$

(corresponding to the damping factors used by Van Driest in equation (1.10) and Cebeci in equation (1.13), respectively) were used with the continuous mixing length formula of equation (4.7). Calculations with both the Cebeci-Smith procedure and the present procedure yielded virtually identical skin friction distributions for this case. The calculations made using equation (4.9) for A gave very slightly better agreement with the experimental results and are shown in Figure 4-4.

Also shown in Figure 4-4 is the skin friction distribution calculated for an equilibrium flow with $\beta=5.4$. For this calculation, the freestream velocity downstream of the initial station and the freestream velocity gradient everywhere were obtained from the requirement that $\beta=5.4$ everywhere. The resulting freestream velocity distribution was also in very good agreement with the experimental one.

4.2.3 Tests of Present Procedure for Flow 2500

Following the significant improvement in the calculated skin friction distribution obtained for Flow 2600, the procedure was applied to the mild adverse pressure gradient flow of Bradshaw [35] with $\beta=1$. Since this flow has a less severe pressure gradient than Flow 2600, the results were not expected to be affected as strongly by the inclusion of

the pressure gradient effect on the inner mixing length constant k_1 . For $\beta=1$, $k_1(\beta)=0.45$, a value not substantially different than the value of 0.4 used in many present mixing length formulas.

For a freestream velocity proportional to x^a (with $a = -0.15$) and also for a freestream velocity chosen to make $\beta=1$ everywhere, calculations were made with the two-piece mixing length formula represented by equation (1.10) in the inner region and

$$l = 0.085\delta \quad (4.11)$$

in the outer region. The two calculations agreed quite well with each other but underpredicted the experimental skin friction distribution by about ten percent, as is shown in Figure 4-5. However, when the calculations were repeated for the continuous mixing length formula of equation (4.7) using A from equation (4.9) and $k_1(\beta)$ from equation (3.1), the resulting skin friction distributions are in much better agreement with the experimental results.

CHAPTER 5

SUMMARY AND CONCLUSIONS

A procedure has been presented for extracting shear stress distributions from measured velocity profile data for two-dimensional, incompressible turbulent boundary layers using the governing partial differential equations expressing the conservation of mass and momentum in the flow. This procedure has been used to obtain shear stress distributions for five equilibrium and one non-equilibrium flows and the corresponding eddy viscosity and mixing length distributions have been calculated.

Uncertainties inherent in the evaluation of the velocity derivative in the flow direction, both in and outside the boundary layer, have been shown to affect the calculated distributions negligibly near the wall but significantly further away from the wall, with the mixing length distributions least affected.

To determine the shear stress distribution through the boundary layer, the freestream velocity and velocity gradient and the wall shear stress must be known. However, these quantities cannot be chosen independently if the shear stress is to approach zero at the edge of the boundary layer as is observed experimentally. The values of the wall shear stress

which must be used with a given freestream velocity gradient in order to make the shear stress approach zero at the edge of the boundary layer are frequently unreasonable. If the Ludwig-Tillmann skin friction formula is used to give the wall shear stress for a given freestream velocity gradient, the shear stress usually does not approach zero at the edge of the boundary layer. However, the calculated distributions agree exceptionally well with available experimental results if the Ludwig-Tillmann formula is used to give the wall shear stress and the freestream velocity gradient is assigned the value which now makes the shear stress approach zero at the edge of the boundary layer.

When this technique is used to improve the values of the freestream velocity gradient, the eddy viscosity and mixing length distributions calculated for each equilibrium boundary layer tend to collapse into a single curve, especially in the wall region. Since the mixing length distributions collapse somewhat better than the eddy viscosity distributions and also are less affected by uncertainties in the velocity derivative as was mentioned above, the mixing length formulation is preferable for use in correlating shear stress distributions for equilibrium boundary layers.

The slope of the mixing length distributions in the wall region for equilibrium turbulent boundary layers increases with increasing values of the pressure gradient parameter β . For β equal to zero, the expected value of 0.4

is obtained for this slope, while for β equal to 5.4, the slope increases to 0.55. This value not only verifies the values derived by Bradshaw and Ferriss from their measured shear stress and velocity profiles, but also verifies the accuracy of their entire experiment.

For nonequilibrium flows in which β is changing rapidly, the slope of the mixing length distribution in the wall region lags significantly behind that expected on the basis of the local value of β , reflecting the upstream history of the flow. This result indicates that the use of a mixing length approach to relate the shear stress distribution to the local velocity profile is not a good approximation unless the mixing length formula is modified to reflect the upstream flow history.

In order to evaluate the effect of the observed dependence of the mixing length on β , calculations were made for the $\beta \approx 5$ equilibrium flow using two completely independent finite-difference boundary layer computation procedures, the very successful Cebeci-Smith procedure and one developed specifically for this study. The results obtained with the two procedures agreed quite well, verifying the accuracy both of the results and of the procedures themselves.

Examination of the calculated results showed that the skin friction distribution was affected greatly by the inclusion of the pressure dependence observed for the inner mixing length constant. When the observed dependence on β was combined with a continuous mixing length formula, the

resulting skin friction distributions agreed almost perfectly with the experimental ones.

Improved results were also obtained when this procedure was applied to the $\beta \approx 1$ equilibrium flow. The procedure used to extract the shear stress distributions from the experimental velocity profile data is a simple, but powerful, technique. Moreover, it is easily extended to more complex flows, such as compressible flows with and without heat and mass transfer. Therefore, the experimentalist should find it useful to provide shear stress, eddy viscosity, and mixing length distributions corresponding to his measured velocity profile distributions and to serve as a check on the two-dimensionality of his flow and the accuracy of his measurements. The theoretician should apply this procedure to successively more complex groups of flows in an effort to develop a mixing length or other eddy viscosity formulation which accurately incorporates all major influences on the flow development.

LIST OF REFERENCES

1. Proceedings - Computation of Turbulent Boundary Layers - 1968 AFOSR-IFP-Stanford Conference, 2 Vols., Stanford Univ., Calif., 1969.
2. Cebeci, T. and Smith, A. M. O., "A Finite-Difference Solution of the Incompressible Turbulent Boundary-Layer Equations by an Eddy-Viscosity Concept," Douglas Aircraft Co. Report No. DAC-67130, 1968.
3. Bradshaw, P., Ferriss, D. H., and Atwell, N. P., "Calculation of Boundary-Layer Development Using the Turbulent Energy Equation," J. Fluid Mech., Vol. 28, Part 3, pp. 593-616, 1967. Also N.P.L. Aero Report 1182, 1966.
4. Boussinesq, J., "Theorie de L'ecoulement tourbillant," Mem. Pres. Acad. Sci., Vol. XXIII, No. 46, Paris, 1877.
5. Prandtl, L., "Uber die Ausgebildete Turbulenz," Z. Angew. Math. Mech., Vol. 5, pp. 136-139, 1925. Also NACA TM 1231, 1949.
6. Schlichting, H., Boundary Layer Theory, McGraw-Hill, N.Y., 6th ed., pp. 545-549, 1968.
7. Bradshaw, P., "Turbulent Boundary Layers," Aero J. Royal Aero. Soc., Vol. 72, pp. 451-459, 1968.
8. Champagne, F. H., Harris, V. G., and Corrsin, S., "Experiments on Nearly Homogeneous Turbulent Shear Flow," J. Fluid Mech., Vol. 41, Part 1, pp. 81-139, 1970.
9. Cebeci, T., Smith, A. M. O., and Mosinskis, G., "Calculation of Compressible Adiabatic Turbulent Boundary Layers," AIAA Paper No. 69-687, 1969.

10. Cebeci, T. and Mosinskis, G., "Calculation of Heat and Mass Transfer in Turbulent Flows at Low Mach Numbers," Douglas Aircraft Co. Report No. DAC-70015, 1969.
11. Cebeci, T., "Calculation of Compressible Turbulent Boundary Layers with Heat and Mass Transfer," AIAA Paper No. 70-741, 1970.
12. Cebeci, T. and Smith, A. M. O., "A Finite-Difference Method for Calculating Compressible Laminar and Turbulent Boundary Layers," J. Basic Eng., Vol. 92, No. 3, pp. 523-535, 1970.
13. Cebeci, T., "Behavior of Turbulent Flow near a Porous Wall with Pressure Gradient," AIAA J., Vol. 8, No. 12, pp. 2152-2156, 1970.
14. Keller, H. B. and Cebeci, T., "Accurate Numerical Methods for Boundary Layer Flows - II. Two-Dimensional Turbulent Flows," AIAA Paper No. 71-164, 1971.
15. Cebeci, T. and Mosinskis, G. J., "Computation of Incompressible Turbulent Boundary Layers at Low Reynolds Numbers," AIAA J., Vol. 9, No. 8, pp. 1632-1634, 1971.
16. Van Driest, E. R., "On Turbulent Flow Near a Wall," J. Aero. Sci., Vol. 23, No. 11, pp. 1007-1011, 1956.
17. Clauser, F. H., "The Turbulent Boundary Layer," Adv. Appl. Mech., Vol. IV, pp. 1-51, 1956.
18. Klebanoff, P. S., "Characteristics of Turbulence in a Boundary Layer with Zero Pressure Gradient," NACA Report 1247, 1956.
19. Chi, S. W. and Chang, C. C., "Effective Viscosity in a Turbulent Boundary Layer," AIAA J., Vol. 7, No. 10, pp. 2032-2045, 1969.
20. Coles, D., "The Law of the Wake in the Turbulent Boundary Layer," J. Fluid Mech., Vol. 1, pp. 191-226, 1956.

21. Kays, W. M., "Heat Transfer to the Transpired Boundary Layer," ASME Paper No. 71-HT-44, 1971.
22. Bradshaw, P. and Ferriss, D. H., "The Response of a Retarded Equilibrium Turbulent Boundary Layer to the Sudden Removal of Pressure Gradient," N.P.L. Aero Report 1145, 1965.
23. Schultz-Grunow, F., "New Frictional Resistance Law for Smooth Plates," NACA TM 986, 1941.
24. Wieghardt, K. and Tillmann, W., "On the Turbulent Friction for Rising Pressure," NACA TM 1314, 1951.
25. Escudier, M. P., "The Distribution of the Mixing Length in Turbulent Flows near Walls," Imperial College, Mech. Eng. Dept. Report TWF/TN/1, 1965.
26. Spence, D. A., "Distributions of Velocity, Enthalpy and Shear Stress in the Compressible Turbulent Boundary Layer on a Flat Plate," R.A.E. Rept. No. Aero. 2631, 1959.
27. Maise, G. and McDonald, H., "Mixing Length and Kinematic Eddy Viscosity in a Compressible Boundary Layer," AIAA J., Vol. 6, No. 1, 1968.
28. Poe, G. G. and Holsen, J. N., "Shear Stress Distributions in Turbulent Compressible Boundary Layers," Washington Univ., Dept. Chem. Eng. Tech. Note, June, 1968.
29. Meier, H. U. and Rotta, J. C., "Experimental and Theoretical Investigations of Temperature Distributions in Supersonic Boundary Layers," AIAA Paper No. 70-744, 1970.
30. Bushnell, D. M. and Morris, D. J., "Eddy Viscosity Distributions in a Mach 20 Turbulent Boundary Layer," AIAA J., Vol. 9, No. 4, pp. 764-766, 1971.
31. Bushnell, D. M. and Morris, D. J., "Shear-Stress, Eddy-Viscosity, and Mixing-Length Distributions in Hypersonic Turbulent Boundary Layers," NASA TM X-2310, 1971.

32. Clauser, F. H., "Turbulent Boundary Layers in Adverse Pressure Gradients," J. Aero. Sci., Vol. 21, pp. 91-108, 1954.
33. Townsend, A. A., "Equilibrium Layers and Wall Turbulence," J. Fluid Mech., Vol. 11, pp. 97-120, 1961.
34. Mellor, G. I. and Gibson, D. M., "Equilibrium Turbulent Boundary Layers," J. Fluid Mech., Vol. 24 Pt. 2, pp. 225-253, 1966.
35. Bradshaw, P., "The Turbulence Structure of Equilibrium Boundary Layers," N.P.L. Aero Report 1184, 1966.
36. Herring, H. J. and Norbury, J. F., "Some Experiments on Equilibrium Turbulent Boundary Layers in Favourable Pressure Gradients," J. Fluid Mech., Vol. 27, Pt. 3, pp. 541-549, 1967.
37. Spalding, D. B., "A Single Formula for the Law of the Wall," J. Appl. Mech., Vol. 28, pp. 455-458, 1961.
38. Glowacki, W. J., "Analytical Procedures Used to Obtain and Evaluate the Eddy Viscosity and Mixing Length Extracted from Incompressible Turbulent Boundary Layer Data," NOLTR 74-106, 1974.
39. Ludwig, H. and Tillmann, W., "Investigations of the Wall Shearing Stress in Turbulent Boundary Layers," NACA TM 1285, 1950.
40. Spalding, D. B. and Chi, S. W., "The Drag of a Compressible Turbulent Boundary Layer on a Smooth Flat Plate With and Without Heat Transfer," J. Fluid Mech., Vol. 18, pp. 117-143, 1964.

41. Glowacki, W. J. and Chi, S. W., "Effect of Pressure Gradient on Mixing Length for Equilibrium Turbulent Boundary Layers," AIAA Paper No. 72-213, 1972.
42. Chi, S. W. and Glowacki, W. J., "Applicability of Mixing Length Theory to Turbulent Boundary Layers Beneath Intense Vortices," J. Appl. Mech., Vol. 41, No. 1, pp. 15-19, 1974. Also ASME Paper No. 73-WA/APM-24, 1973.

TABLE 2-1

DIMENSIONLESS WALL SHEAR STRESSES (C_f) FROM VARIOUS SOURCES

	PROFILE NUMBER	MEASURED VALUE	LUDWIG- TILLMANN	LAW OF WALL	LAW OF WAKE
FLOW 2400	2401	.00135	.001372	.001405	.001261
BRADSHAW-FERRISS	2402	.00139	.001382	.001419	.001263
RELAXING FLOW	2403	.00149	.001447	.001515	.001345
($\beta=5.0$)	2404	.00167	.001565	.001695	.001441
	2405	.00173	.001680	.001856	.001577
	2406	.00183	.001806	.002005	.001710
	2407	.00192	.001894	.002105	.001828
FLOW 2500	2501	.00224	.002370	.00230	.002210
BRADSHAW	2502	.00211	.002140	.00218	.002127
EQUILIBRIUM FLOW	2503	.00203	.002000	.00205	.002003
($\beta=1$)	2504	.00183	.001893	.00195	.001905
FLOW 2600	2601	.00145	.001419	.00142	.001239
BRADSHAW-FERRISS	2602	.00132	.001359	.00138	.001267
EQUILIBRIUM FLOW	2603	.00125	.001366	.00139	.001289
($\beta=5$)	2604	.00123	.001273	.00132	.001226
FLOW 2700	2701	.00343*	.003447	.00339	.003349
HERRING-NORBURY	2702	.00344*	.003422	.00338	.003329
EQUILIBRIUM FLOW	2703	.00359*	.003645	.00352	.003507
($\beta=-0.35$)	2704	.00353*	.003634	.00352	.003520
	2705	.00353*	.003521	.00346	.003454
	2706	.00345*	.003416	.00340	.003377
FLOW 2800	2801	.00334*	.003271	.00327	.003215
HERRING-NORBURY	2802	.00341*	.003378	.00333	.003285
EQUILIBRIUM FLOW	2803	.00360*	.003516	.00350	.003496
($\beta=-0.53$)	2804	.00375*	.003677	.00367	.003691
	2805	.00382*	.003702	.00375	.003771
FLOW 1400	1414	-	.002693	.00269	.002663
WIEGHARDT	1415	-	.002652	.00266	.002630
ZERO PRESSURE	1416	-	.002661	.00260	.002591
GRADIENT FLOW	1417	-	.002617	.00260	.002568
($\beta=0$)	1418	-	.002574	.00256	.002519
	1419	-	.002537	.00253	.002488
	1420	-	.002506	.00247	.002469
	1421	-	.002454	.00247	.002431
	1422	-	.002423	.00246	.002435
	1423	-	.002398	.00243	.002422

Note: Law of Wall and Law of Wake Values are Taken from Coles [1]

*Calculated using Mellor-Gibson Theory [34].

TABLE 2-2

FREESTREAM VELOCITY AND GRADIENTS USED

	PROFILE NUMBER	VELOCITY u_e (FT/SEC)	ORIGINAL* du_e/dx (SEC ⁻¹)	FINAL† du_e/dx (SEC ⁻¹)	% CHANGE
FLOW 2400	2401	114.51	-5.80	-7.9746	-37.5
BRADSHAW-FERRISS	2402	111.65	-4.00	-4.1660	-4.2
RELAXING FLOW	2403	110.05	-2.20	-1.3778	+37.4
($\beta \approx 5 \rightarrow 0$)	2404	110.00	-0.50	0.4514	+190.
	2405	110.00	0.	0.5447	-
	2406	110.00	0.	-0.0480	-
	2407	110.00	0.	0.1716	-
FLOW 2500	2501	143.42	-10.34	-13.0670	-26.4
BRADSHAW	2502	129.22	-4.66	-5.2404	-12.5
EQUILIBRIUM FLOW	2503	123.47	-3.55	-3.9068	-10.1
($\beta \approx 1$)	2504	118.98	-2.69	-3.1747	-18.0
FLOW 2600	2601	136.51	-17.98	-30.9237	-72.0
BRADSHAW-FERRISS	2602	113.78	-7.33	-5.9336	+19.1
EQUILIBRIUM FLOW	2603	104.93	-4.89	-4.7041	+3.8
($\beta \approx 5$)	2604	98.39	-3.58	-4.0545	-13.3
FLOW 2700	2701	76.50	2.65	3.1862	+20.2
HERRING-NORBURY	2702	79.80	4.90	5.3341	+8.9
EQUILIBRIUM FLOW	2703	84.60	6.13	7.6231	+24.4
($\beta \approx -0.35$)	2704	90.50	6.20	7.8278	+26.3
	2705	97.10	6.25	7.3178	+17.1
	2706	103.60	6.25	6.6778	+6.8
FLOW 2800	2801	76.90	5.00	3.5122	-29.8
HERRING-NORBURY	2802	82.60	7.30	6.4305	-11.9
EQUILIBRIUM FLOW	2803	90.80	9.50	10.9433	+15.2
($\beta \approx -0.53$)	2804	101.40	12.00	15.8174	+31.8
	2805	115.40	17.00	16.4292	-3.4
FLOW 1400	1414	108.27	0.	0.5119	-
WIEGHARDT	1415	108.27	0.	0.1418	-
ZERO PRESSURE	1416	108.27	0.	0.0978	-
GRADIENT FLOW	1417	108.27	0.	0.0801	-
($\beta = 0$)	1418	108.27	0.	0.1440	-
	1419	108.27	0.	0.1401	-
	1420	108.27	0.	-0.1646	-
	1421	108.27	0.	0.0083	-
	1422	108.27	0.	0.0941	-
	1423	108.27	0.	-0.2633	-

*Original du_e/dx obtained from experimental u_e distribution.†Final du_e/dx obtained from zero freestream shear stress.

TABLE 3-1

PRESSURE GRADIENT PARAMETER β FROM VARIOUS SOURCES

	Profile Number	Experiment	Stanford	Original* du_e/dx	Final† du_e/dx
FLOW 2400	2401	-	4.040	4.030	5.540
BRADSHAW-FERRISS	2402	-	3.026	3.099	3.228
RELAXING FLOW	2403	-	1.637	1.705	1.068
($\beta \approx 5 \rightarrow 0$)	2404	-	0.325	0.349	-0.315
	2405	0.	0.	0.	-0.342
	2406	0.	0.	0.	0.028
	2407	0.	0.	0.	-0.094
FLOW 2500	2501	0.990	0.869	0.929	1.174
BRADSHAW	2502	0.890	0.824	0.868	0.976
EQUILIBRIUM FLOW	2503	0.900	0.858	0.961	1.058
($\beta \approx 1$)	2504	0.915	0.973	0.982	1.159
FLOW 2600	2601	5.100	5.208	5.064	8.710
BRADSHAW-FERRISS	2602	5.480	5.139	5.218	4.224
EQUILIBRIUM FLOW	2603	5.380	4.292	4.779	4.597
($\beta \approx 5$)	2604	5.400	5.172	5.185	5.872
FLOW 2700	2701	-0.229	-0.211	-0.207	-0.249
HERRING-NORBURY	2702	-0.384	-0.388	-0.381	-0.415
EQUILIBRIUM FLOW	2703	-0.355	-0.390	-0.386	-0.481
($\beta = -0.35$)	2704	-0.348	-0.360	-0.349	-0.440
	2705	-0.354	-0.341	-0.337	-0.394
	2706	-0.345	-0.333	-0.331	-0.353
FLOW 2800	2801	-0.548	-0.490	-0.489	-0.343
HERRING-NORBURY	2802	-0.579	-0.634	-0.616	-0.542
EQUILIBRIUM FLOW	2803	-0.620	-0.617	-0.606	-0.698
($\beta = -0.53$)	2804	-0.525	-0.527	-0.513	-0.676
	2805	-0.539	-0.544	-0.535	-0.517
FLOW 1400	1414	0.	0.	0.	-0.058
WIEGHARDT	1415	0.	0.	0.	-0.018
ZERO PRESSURE	1416	0.	0.	0.	-0.013
GRADIENT FLOW	1417	0.	0.	0.	-0.012
($\beta = 0$)	1418	0.	0.	0.	-0.024
	1419	0.	0.	0.	-0.025
	1420	0.	0.	0.	0.031
	1421	0.	0.	0.	-0.002
	1422	0.	0.	0.	-0.021
	1423	0.	0.	0.	0.062

*Original du_e/dx obtained from experimental u_e distribution.†Final du_e/dx obtained from zero freestream shear stress.

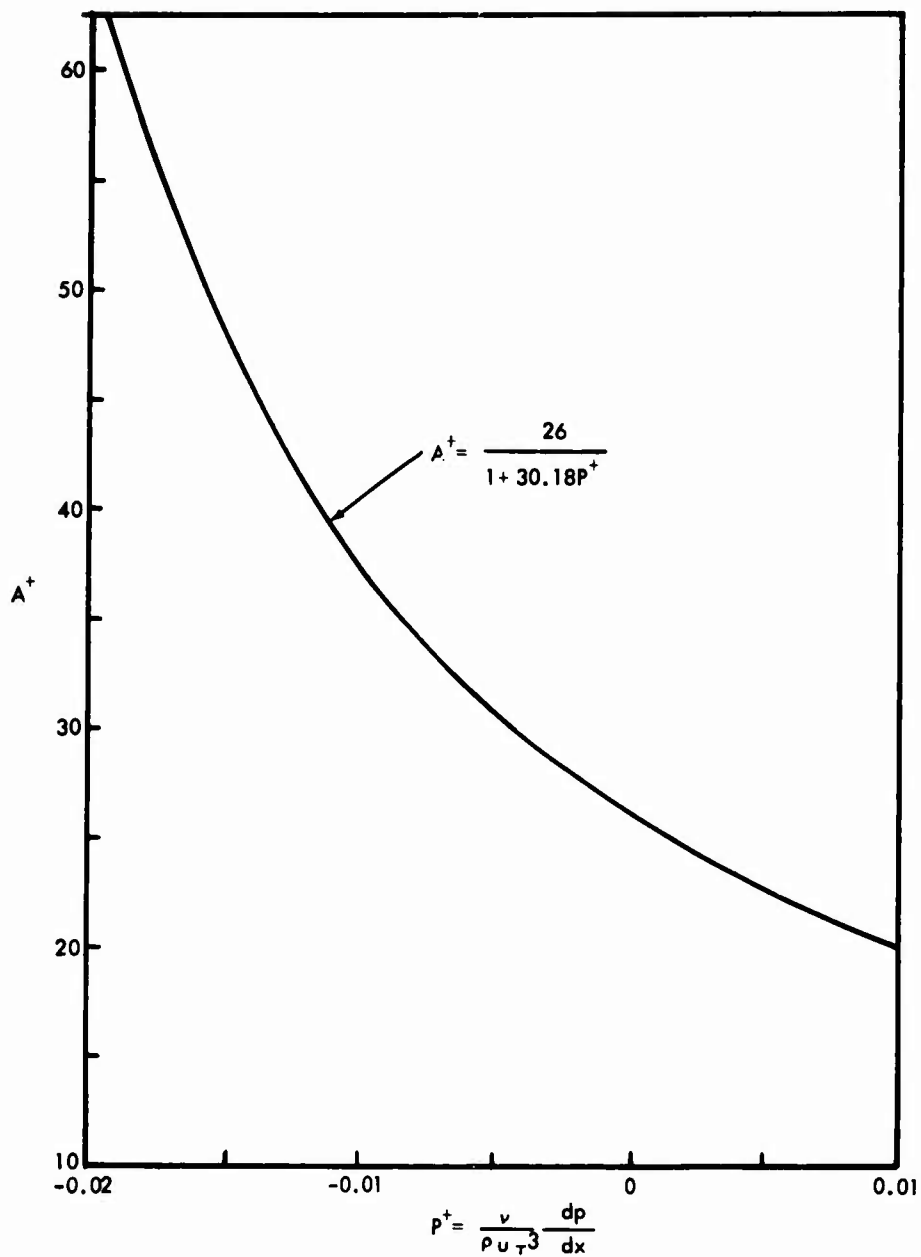


FIG. 1-1 EFFECT OF FREESTREAM PRESSURE GRADIENT ON WALL MIXING LENGTH CONSTANT A^+

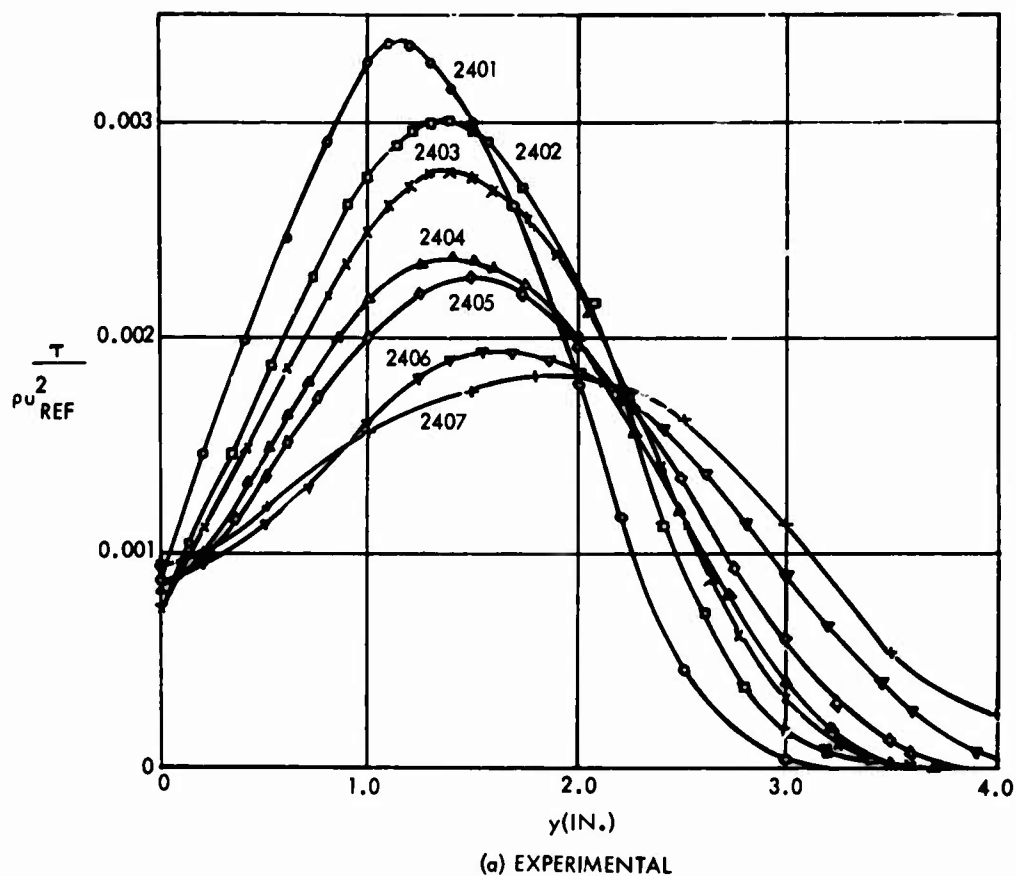
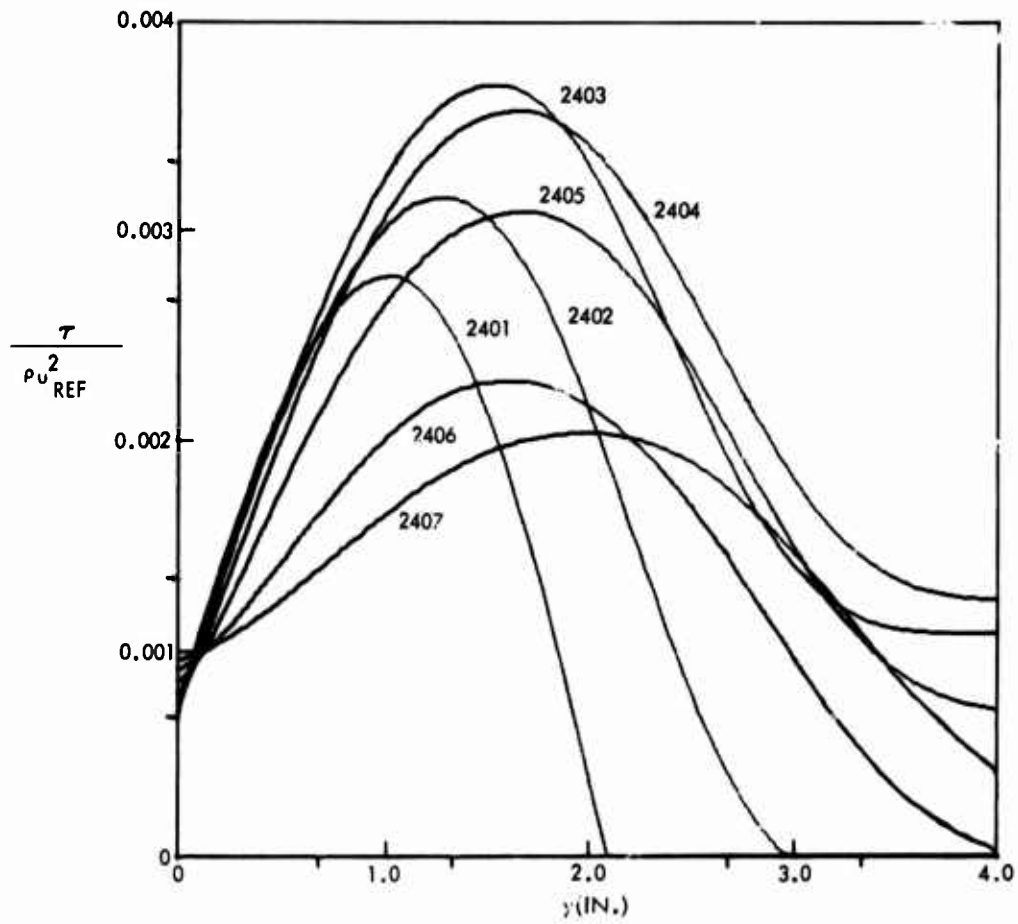
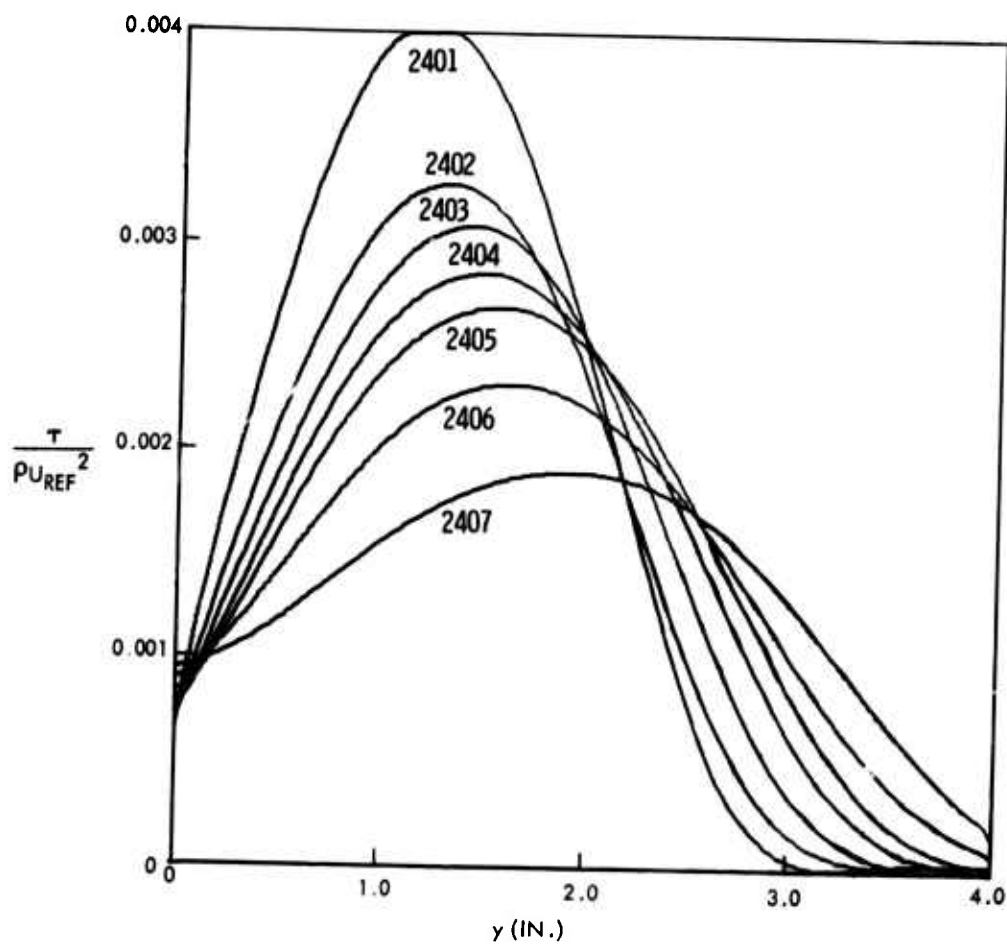


FIG. 3-1 COMPARISON OF EXPERIMENTAL AND CALCULATED SHEAR STRESS DISTRIBUTIONS FOR FLOW 2400, BRADSHAW-FERRISS RELAXING FLOW ($\beta \approx 5 \rightarrow 0$)



(b) CALCULATED USING $\frac{du_e}{dx}$ FROM EXPERIMENTAL DATA

FIG. 3-1 (CONTINUED)



(c) CALCULATED USING $\frac{du_e}{dx}$ FOR ZERO FREESTREAM SHEAR STRESS

FIG. 3-1 (CONTINUED)

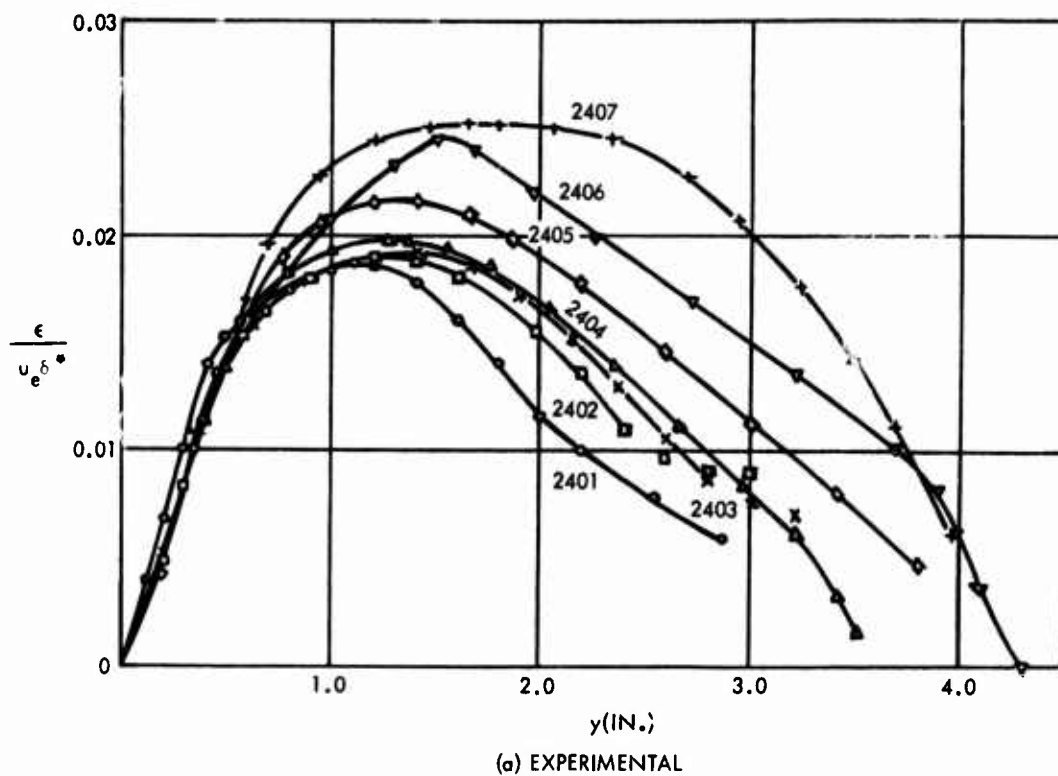
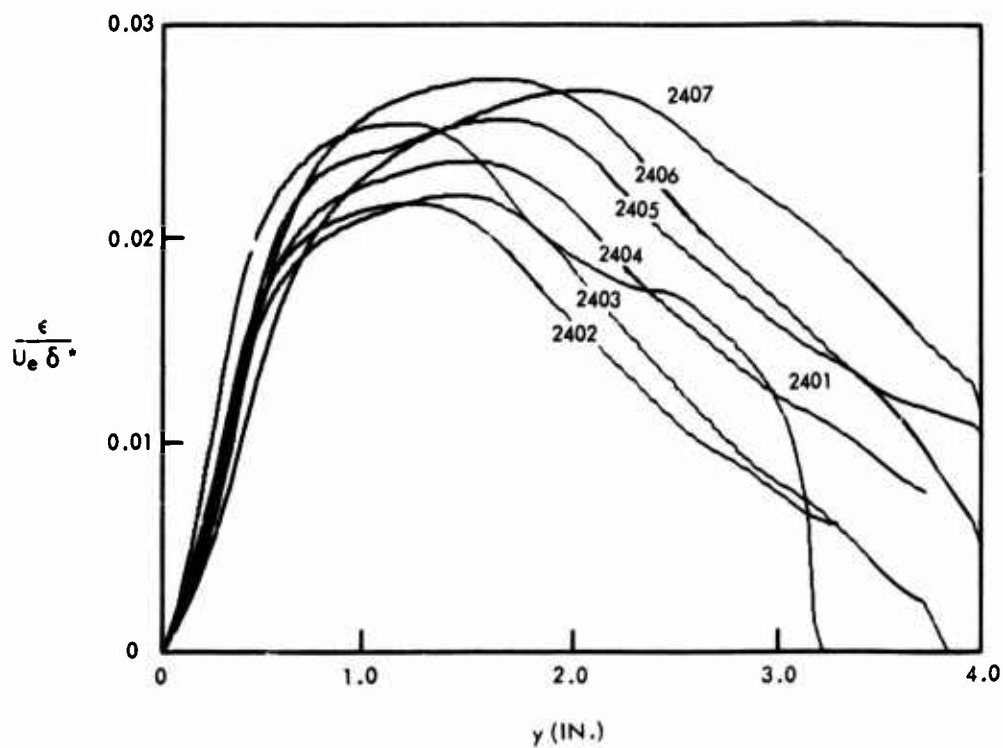


FIG. 3-2 COMPARISON OF EXPERIMENTAL AND CALCULATED EDDY VISCOSITY DISTRIBUTIONS FOR FLOW 2400, BRADSHAW-FERRISS RELAXING FLOW ($\beta \approx 5+0$)



(b) CALCULATED USING $\frac{du_e}{dx}$ FOR ZERO FREESTREAM SHEAR STRESS

FIG. 3-2 (CONTINUED)

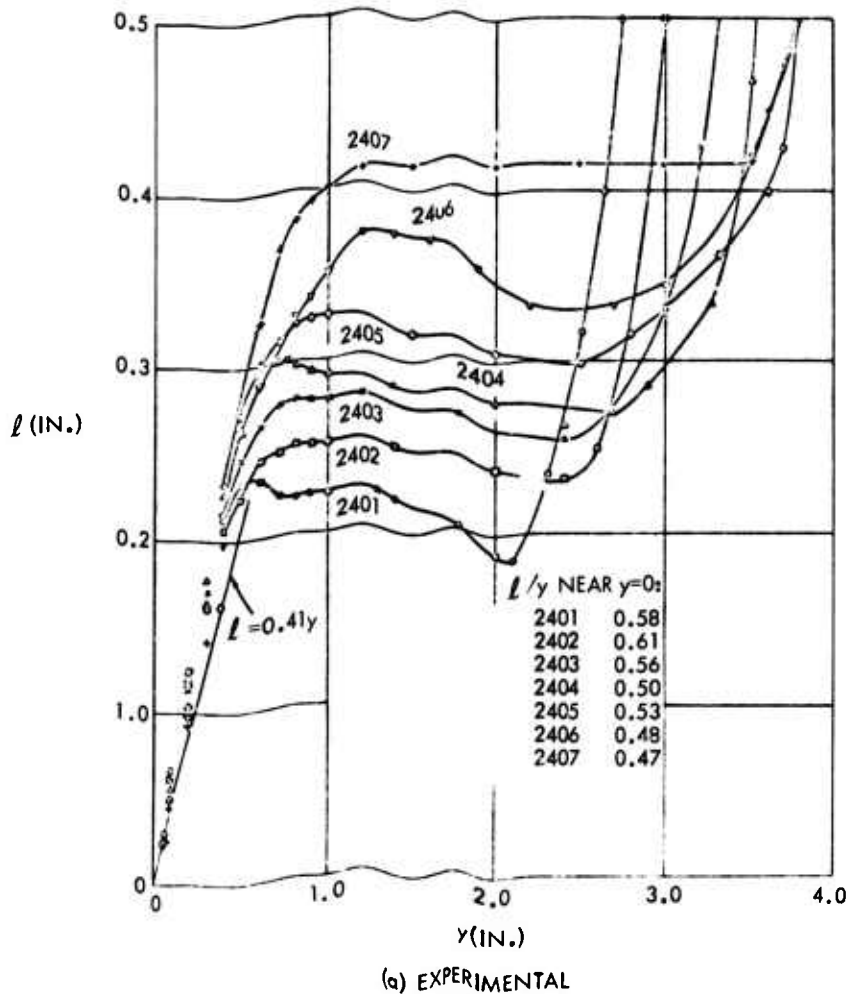
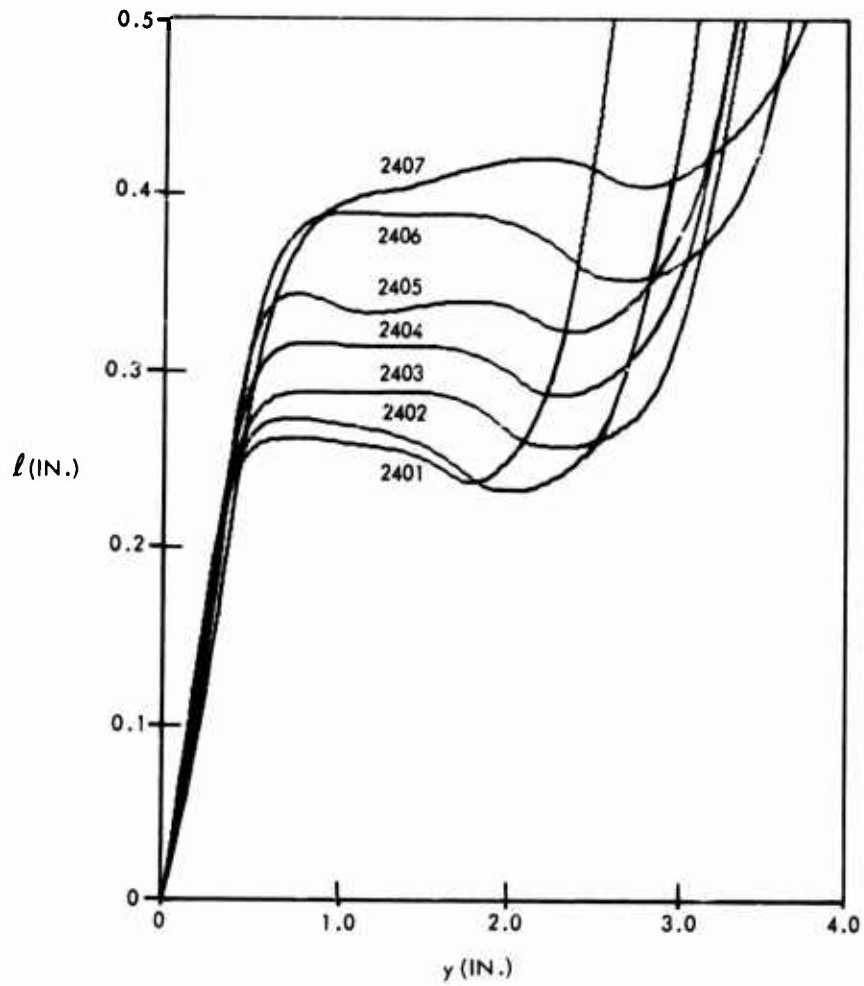


FIG. 3-3 COMPARISON OF EXPERIMENTAL AND CALCULATED MIXING LENGTH DISTRIBUTIONS FOR FLOW 2400, BRADSHAW-FERRISS RELAXING FLOW ($\beta \approx 5 \rightarrow 0$)



(b) CALCULATED USING $\frac{du_e}{dx}$ FOR ZERO FREESTREAM SHEAR STRESS

FIG. 3-3 (CONTINUED)

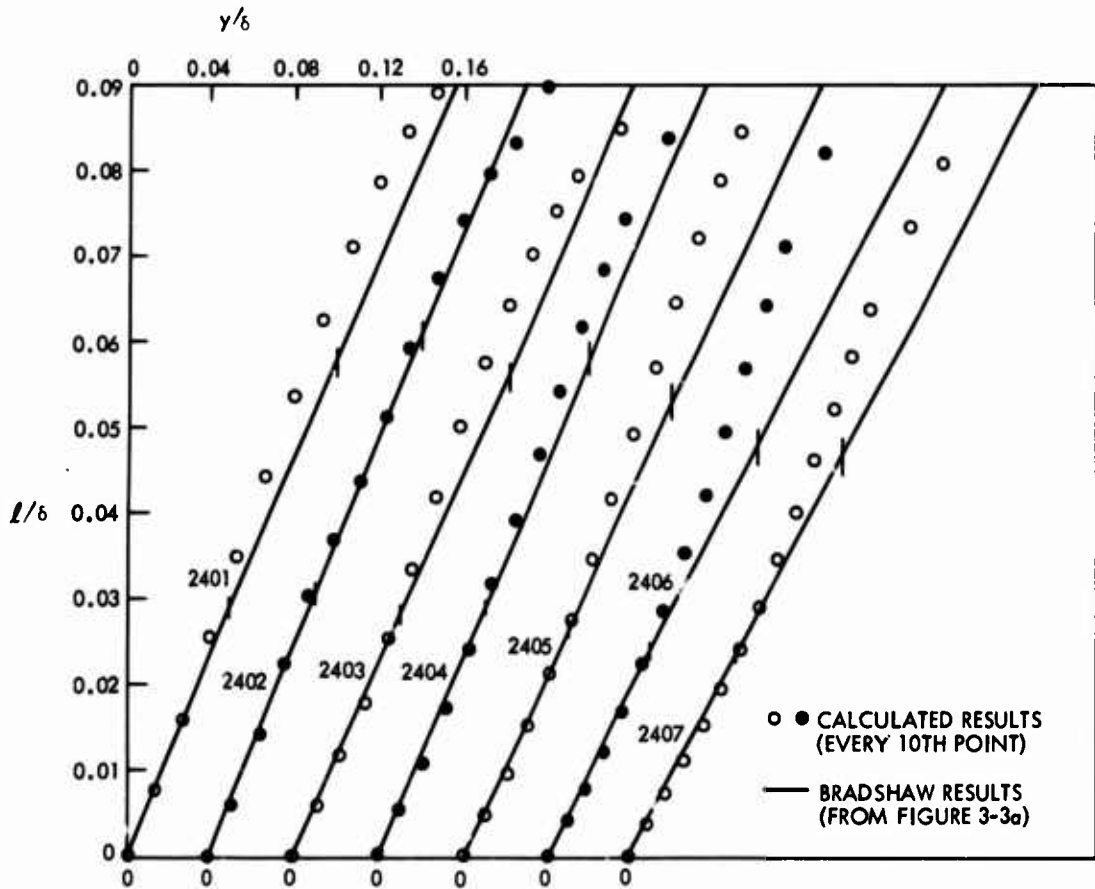


FIG. 3-4 COMPARISONS OF EXPERIMENTAL AND CALCULATED MIXING LENGTH DISTRIBUTIONS IN WALL REGION, FOR FLOW 2400, BRADSHAW-FERRISS RELAXING FLOW ($\beta = 5 \rightarrow 0$)

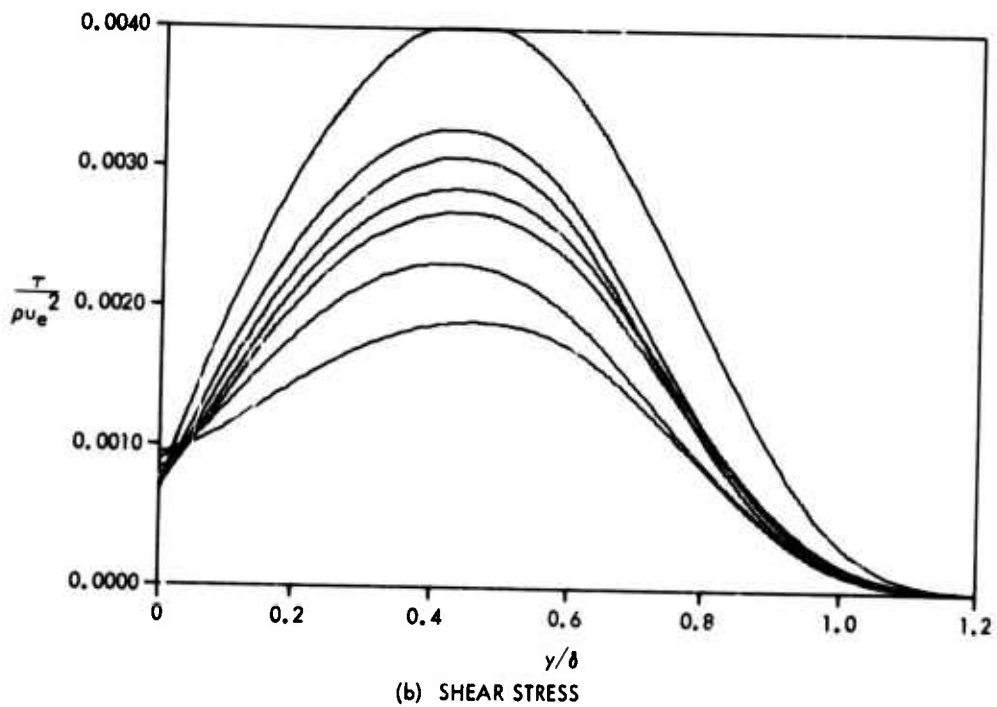
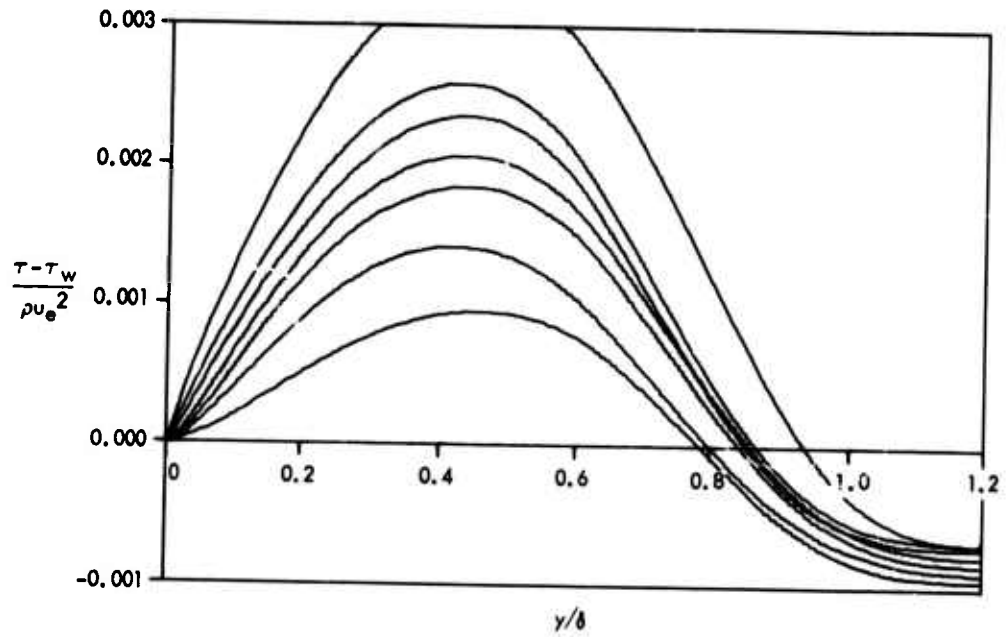
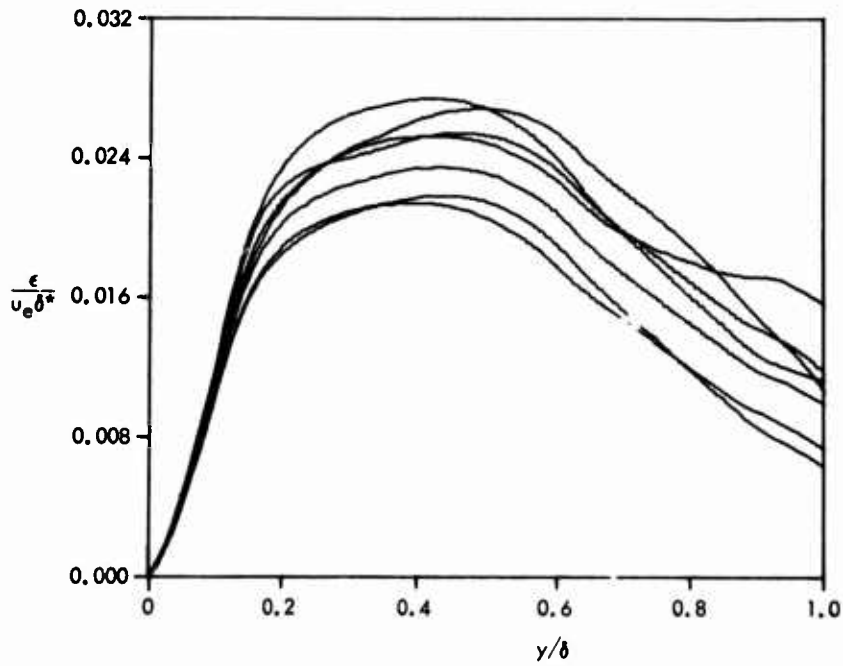
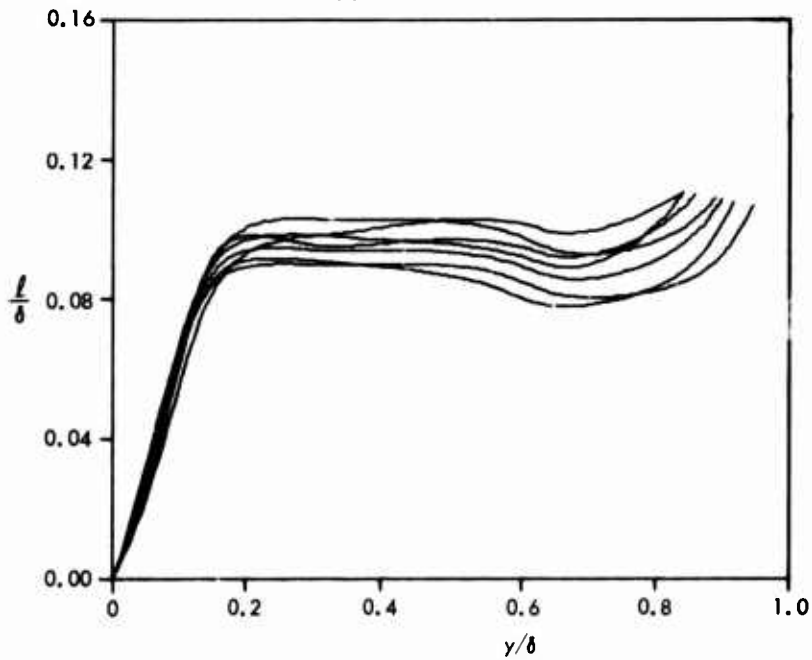


FIG. 3-5 CALCULATED DISTRIBUTIONS FOR FLOW 2400,
BRADSHAW-FERRISS RELAXING FLOW ($\beta \approx 5 \rightarrow 0$)

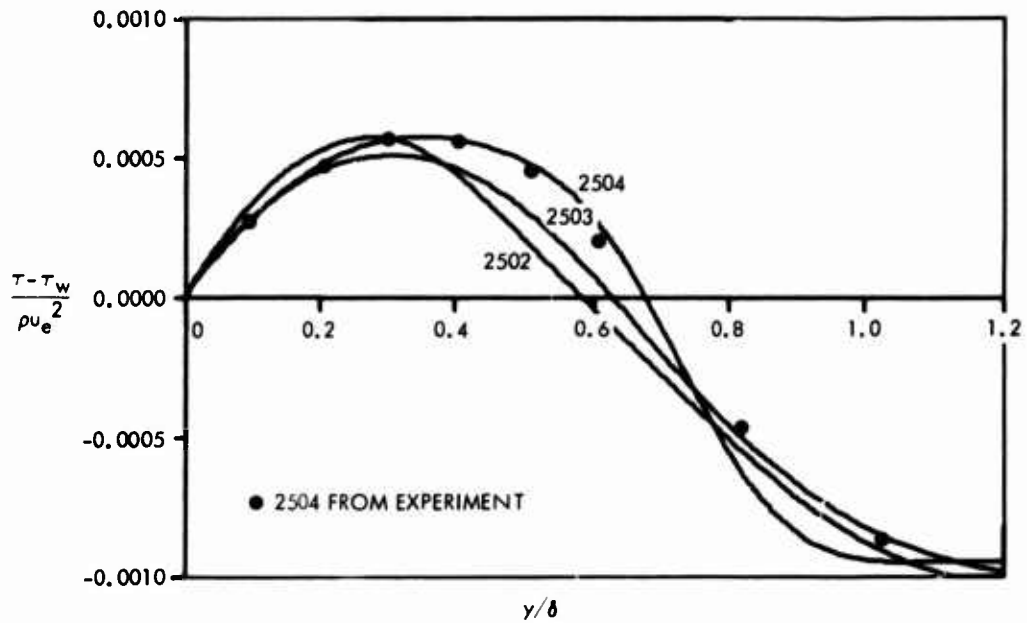


(c) EDDY VISCOSITY

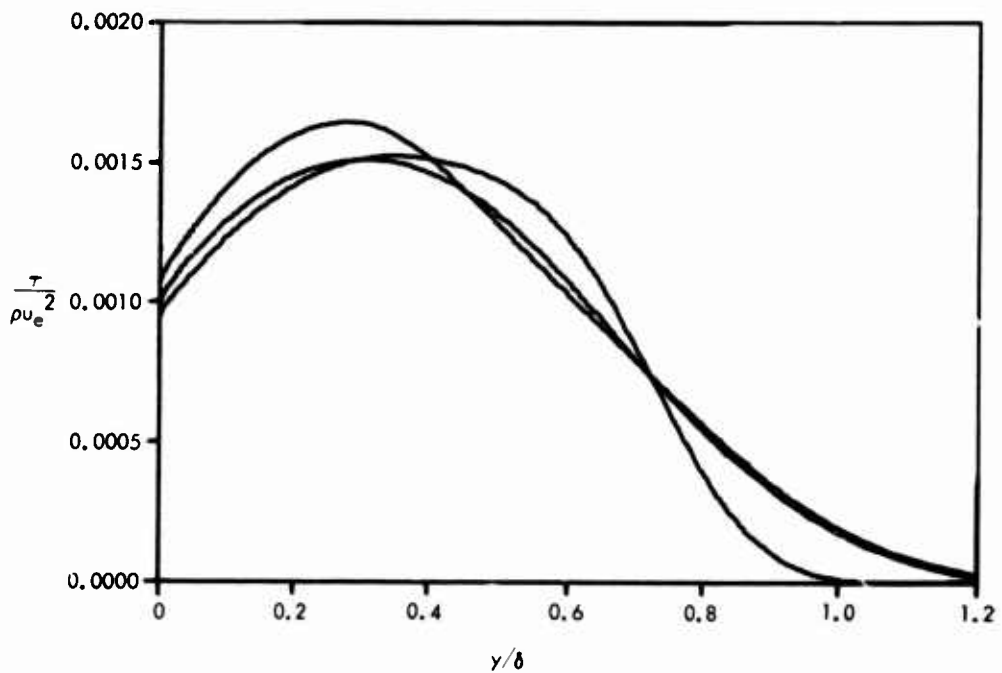


(d) MIXING LENGTH

FIG. 3-5 (CONTINUED)

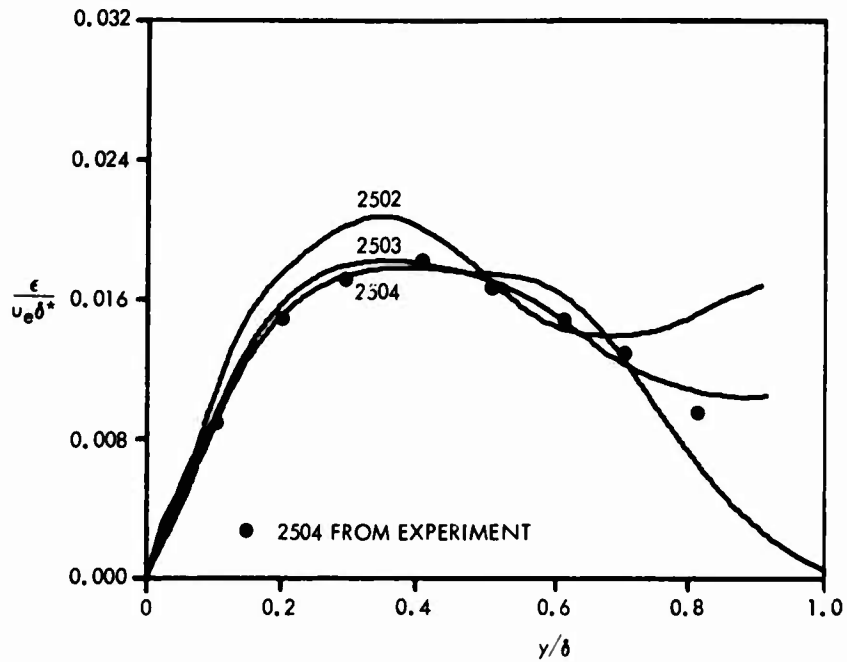


(a) REDUCED SHEAR STRESS

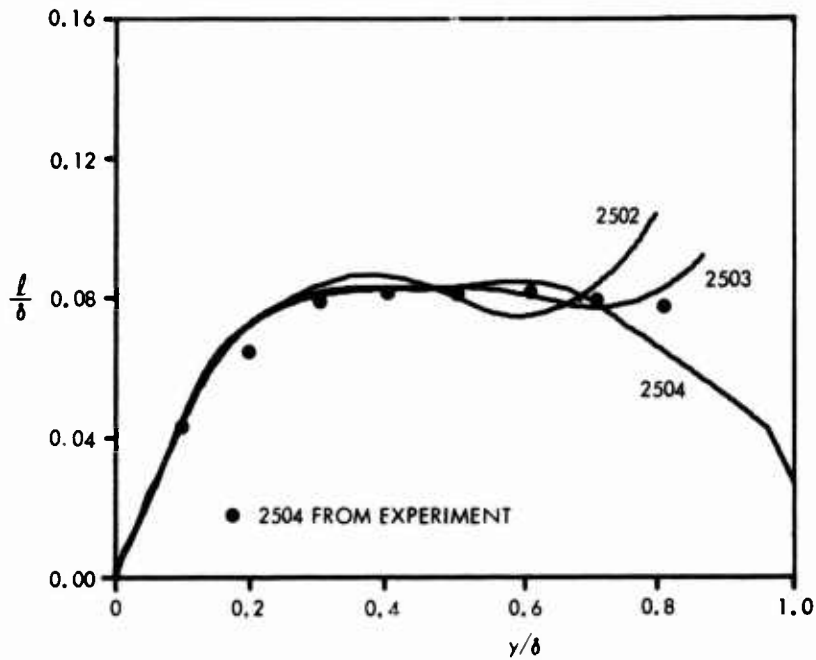


(b) SHEAR STRESS

FIG. 3-6 CALCULATED DISTRIBUTIONS FOR FLOW 2500, BRADSHAW EQUILIBRIUM FLOW ($\beta \approx 1$)

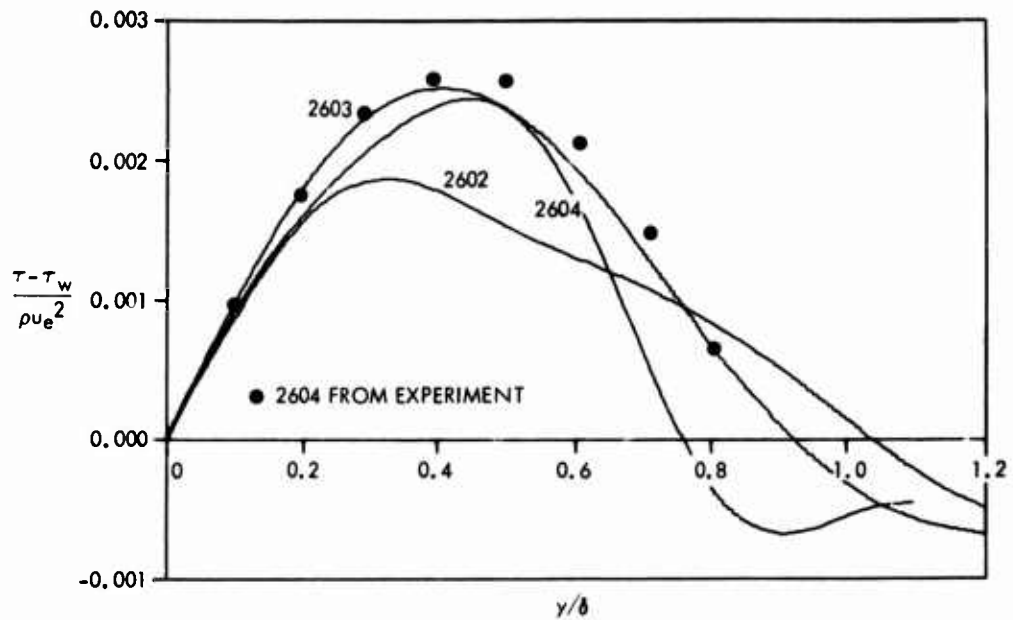


(c) EDDY VISCOSITY

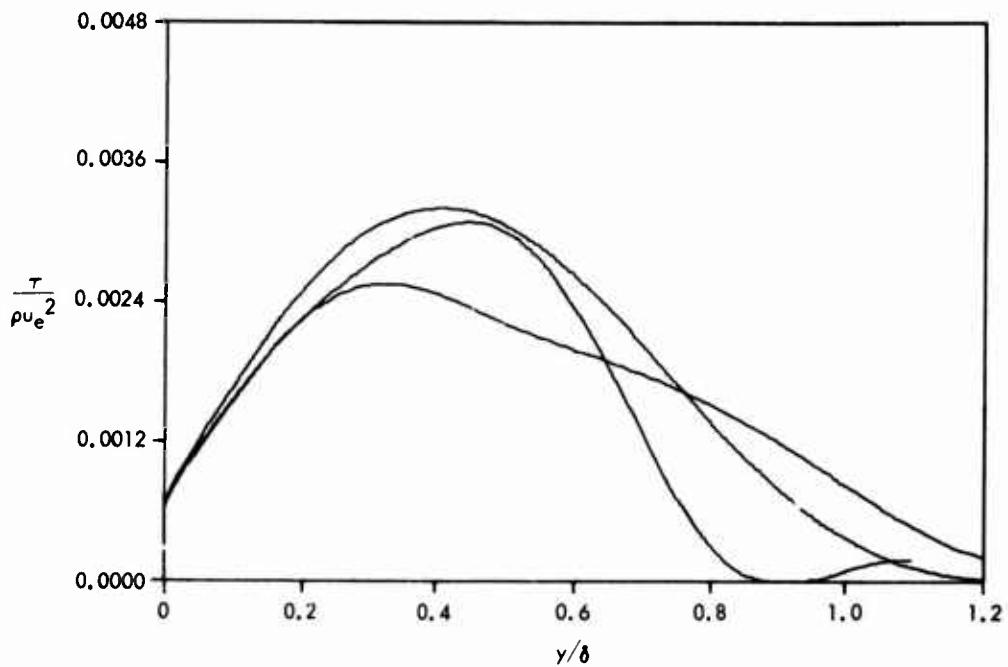


(d) MIXING LENGTH

FIG. 3-6 (CONTINUED)

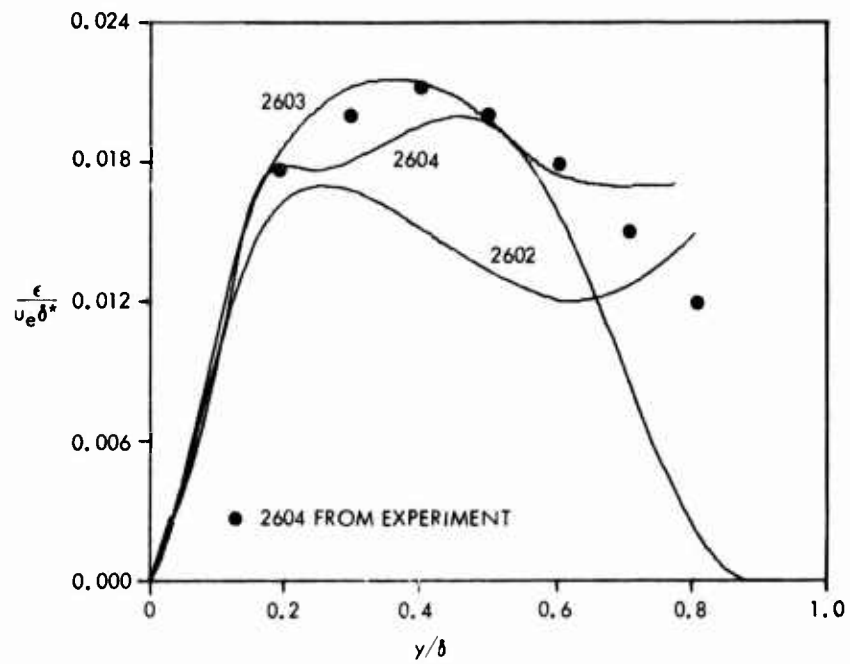


(a) REDUCED SHEAR STRESS

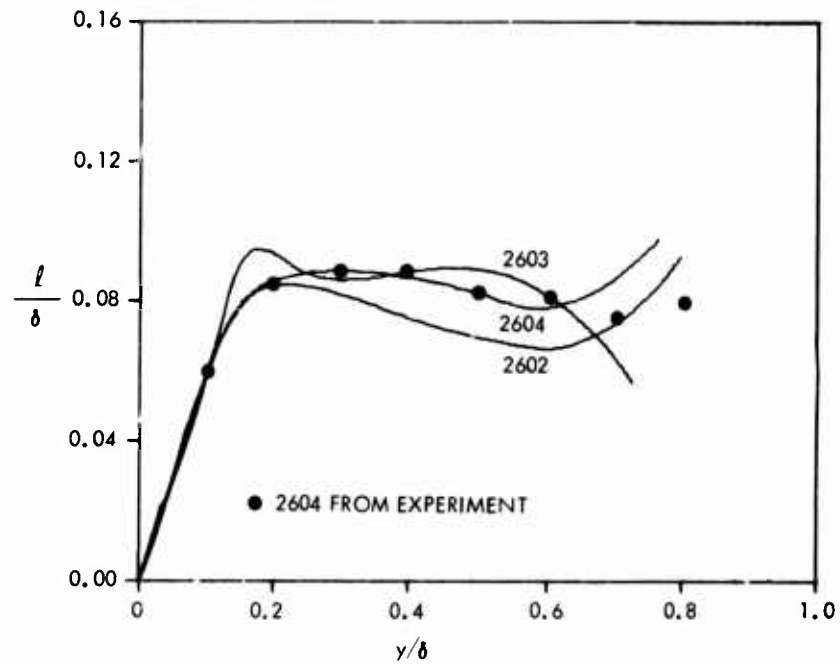


(b) SHEAR STRESS

 FIG. 3-7 CALCULATED DISTRIBUTIONS FOR FLOW 2600,
BRADSHAW - FERRISS EQUILIBRIUM FLOW ($\beta \approx 5$)

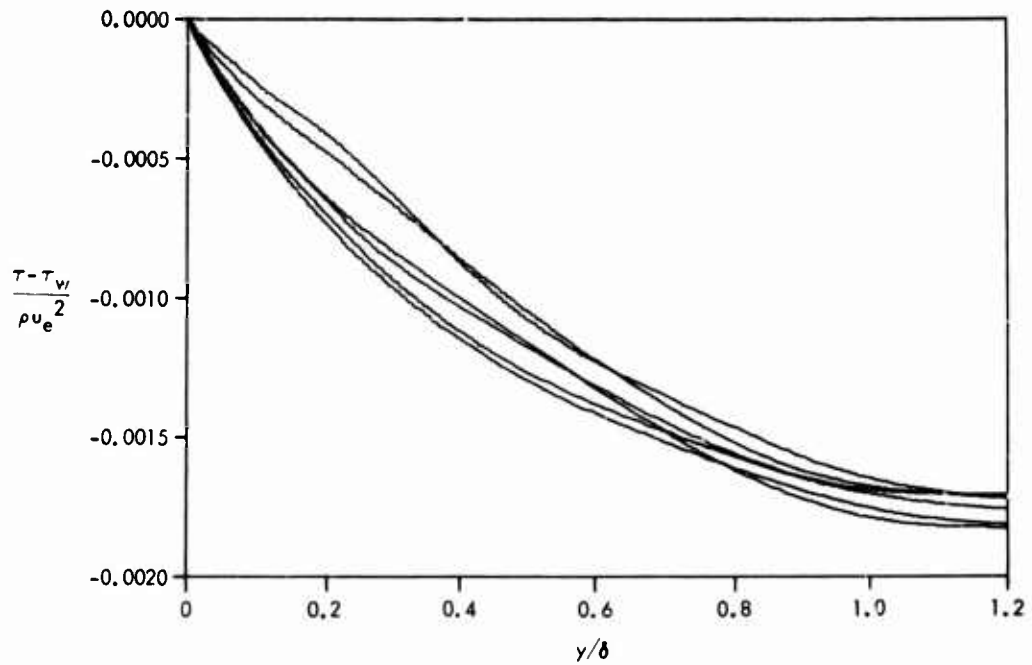


(c) EDDY VISCOSITY

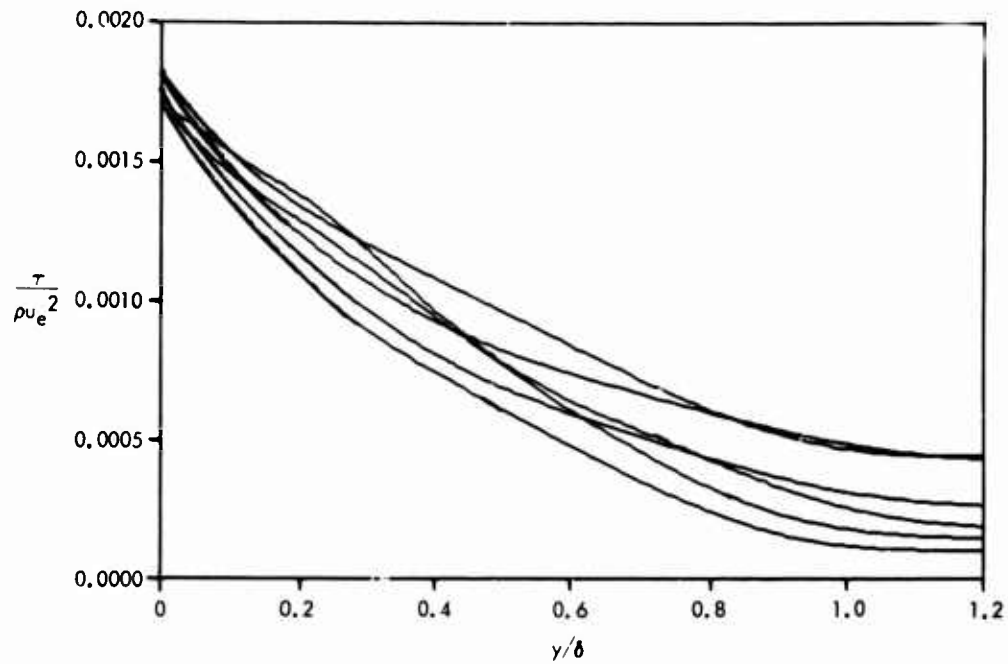


(d) MIXING LENGTH

FIG. 3-7 (CONTINUED)

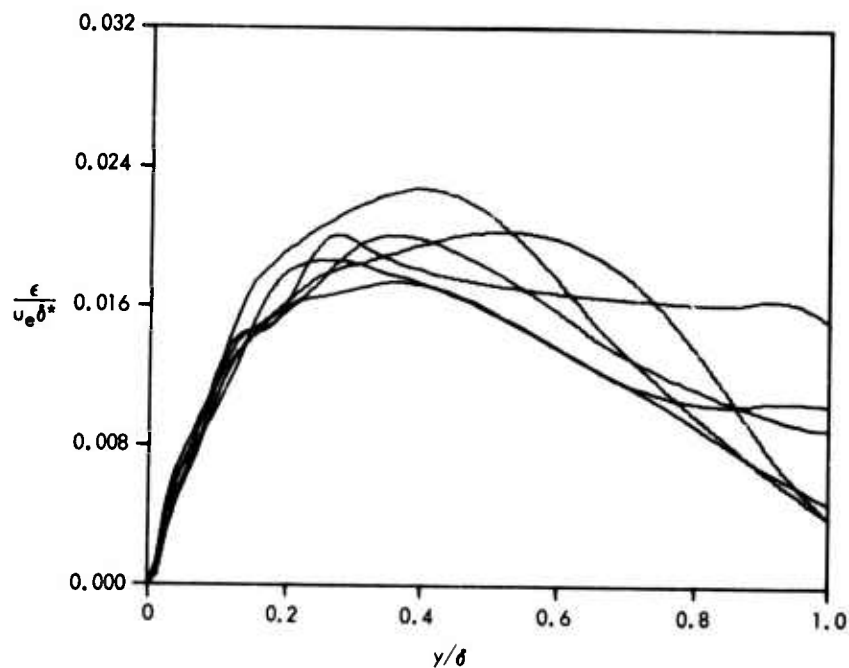


(a) REDUCED SHEAR STRESS

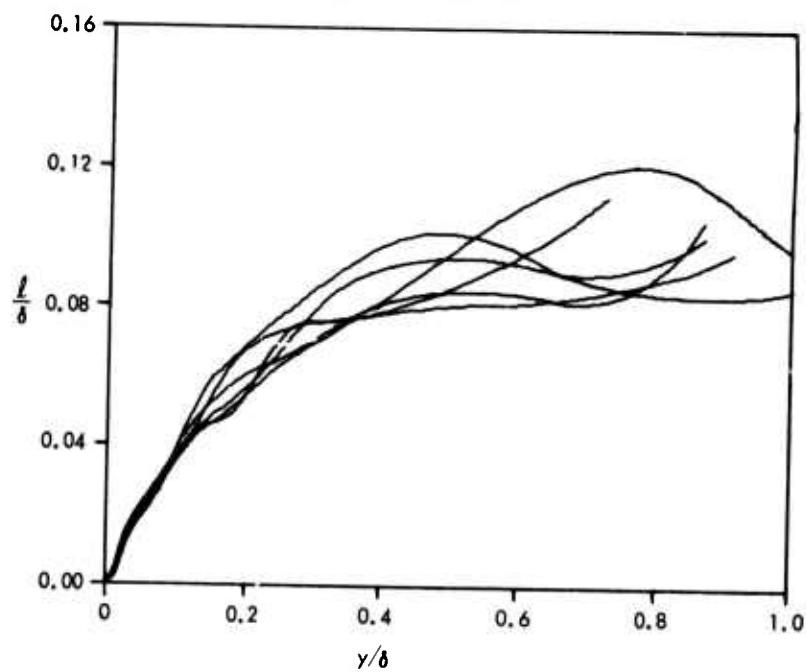


(b) SHEAR STRESS

FIG. 3-8 CALCULATED DISTRIBUTIONS FOR FLOW 2700,
HERRING-NORBURY EQUILIBRIUM FLOW ($\beta = -0.35$)



(c) EDDY VISCOSITY



(d) MIXING LENGTH

FIG. 3-8 (CONTINUED)

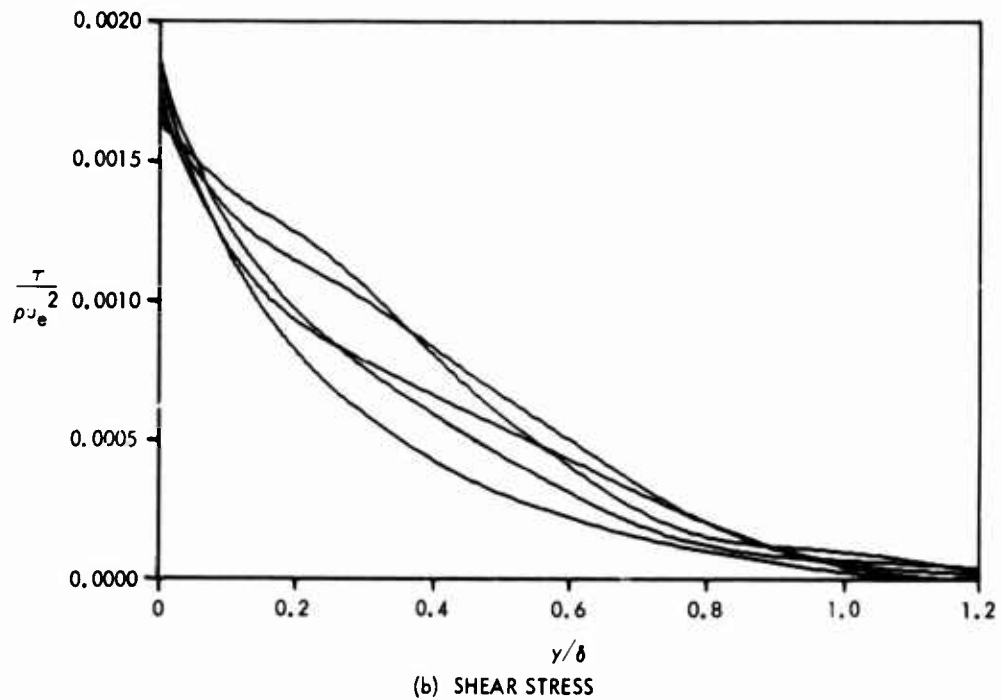
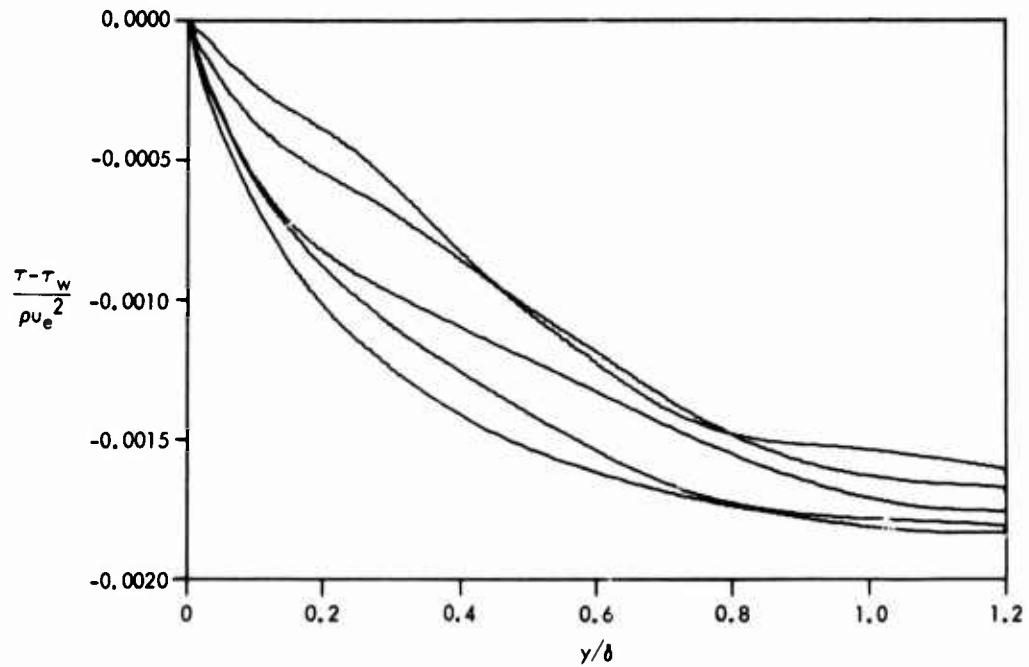
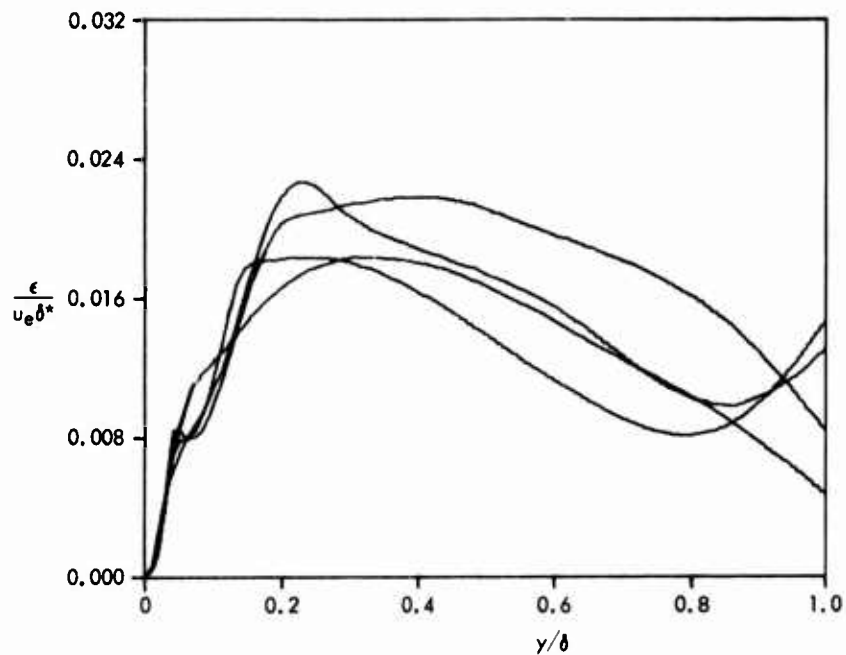
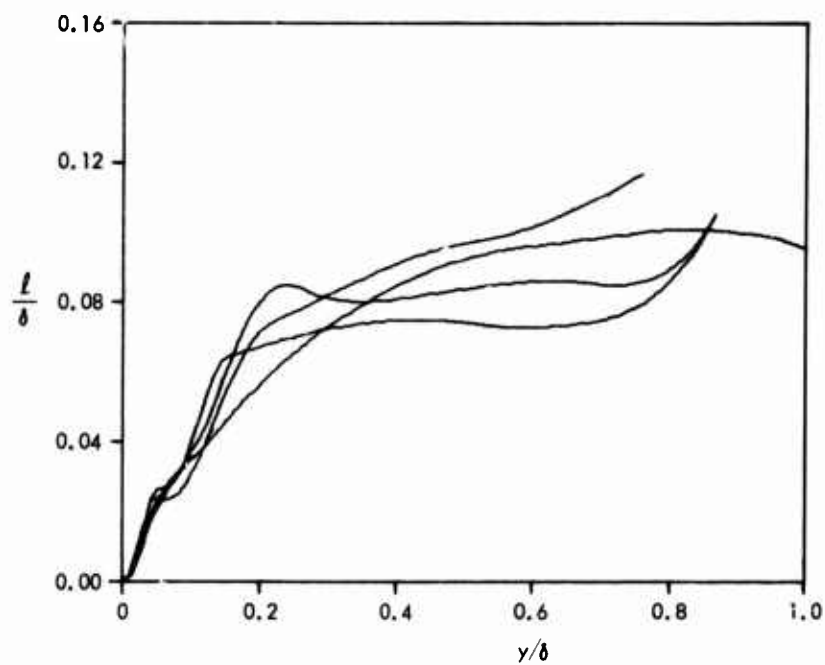


FIG. 3-9 CALCULATED DISTRIBUTIONS FOR FLOW 2800,
HERRING-NORBURY EQUILIBRIUM FLOW ($\beta = -0.53$)

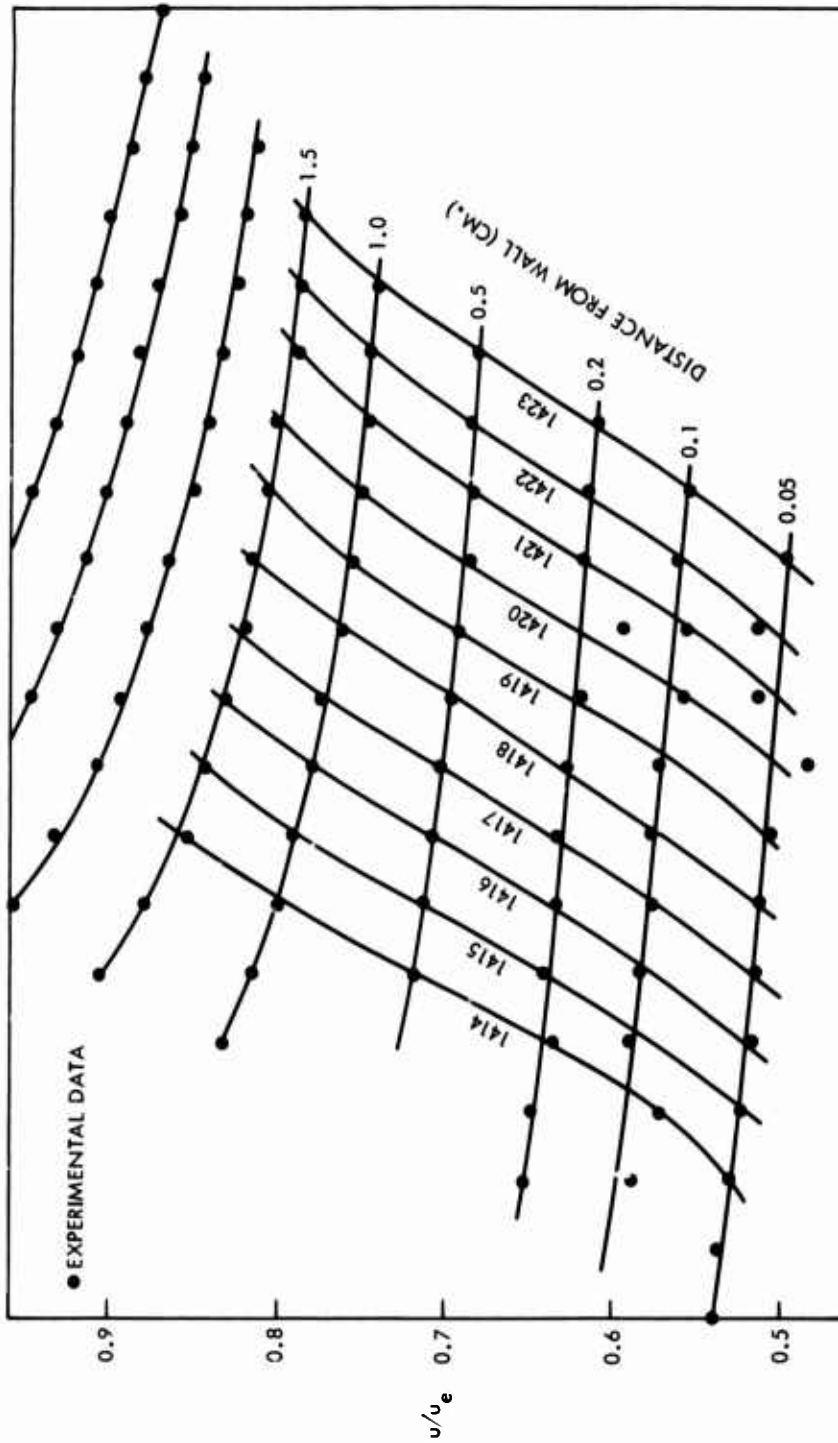


(c) EDDY VISCOSITY



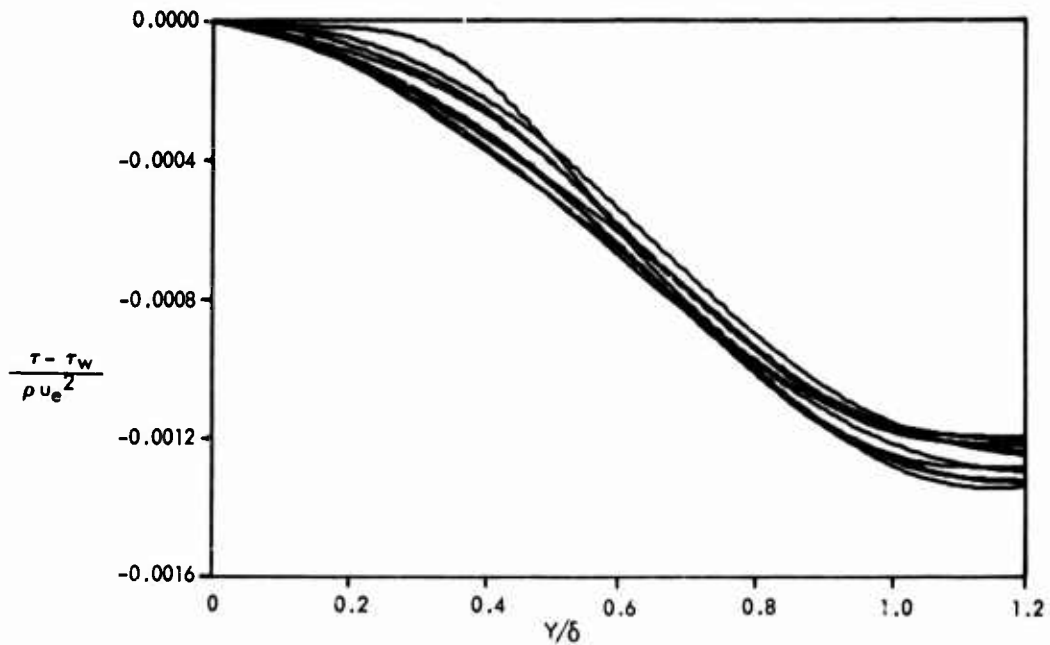
(d) MIXING LENGTH

FIG. 3-9 (CONTINUED)

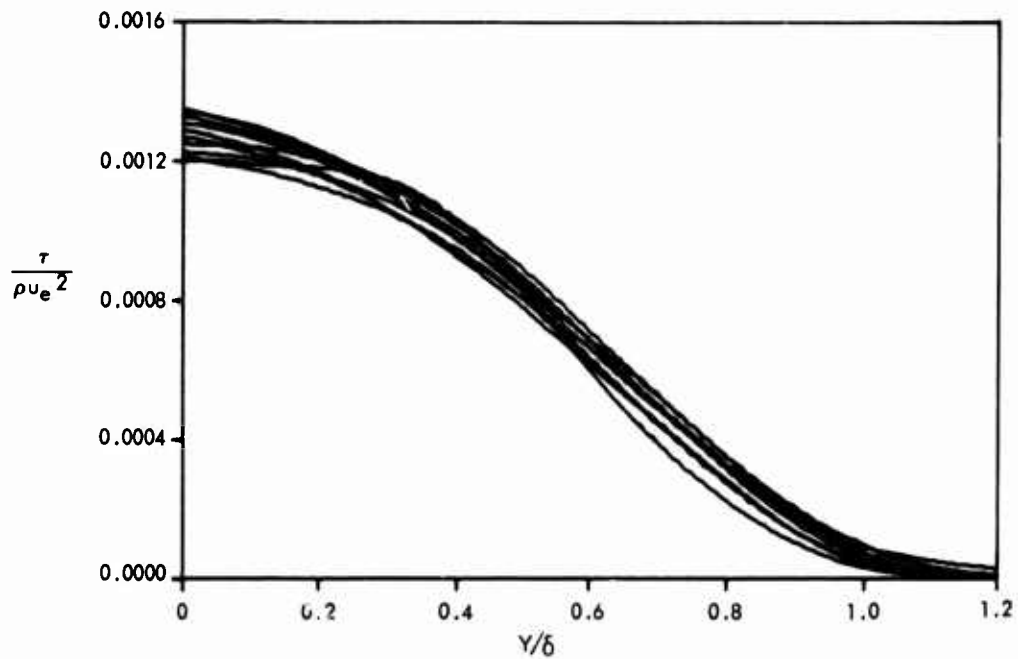


PROFILE STATION

FIG. 3-10 VELOCITY DISTRIBUTIONS IN WALL REGION FOR FLOW 1400, WIEGHARDT-TILLMANN ZERO PRESSURE GRADIENT FLOW ($\beta=0$)

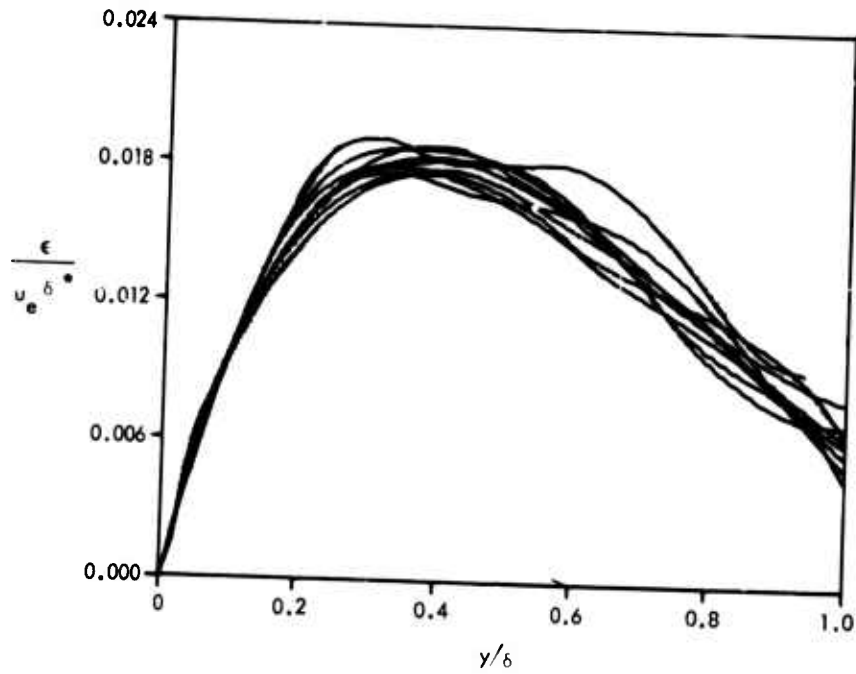


(a) REDUCED SHEAR STRESS

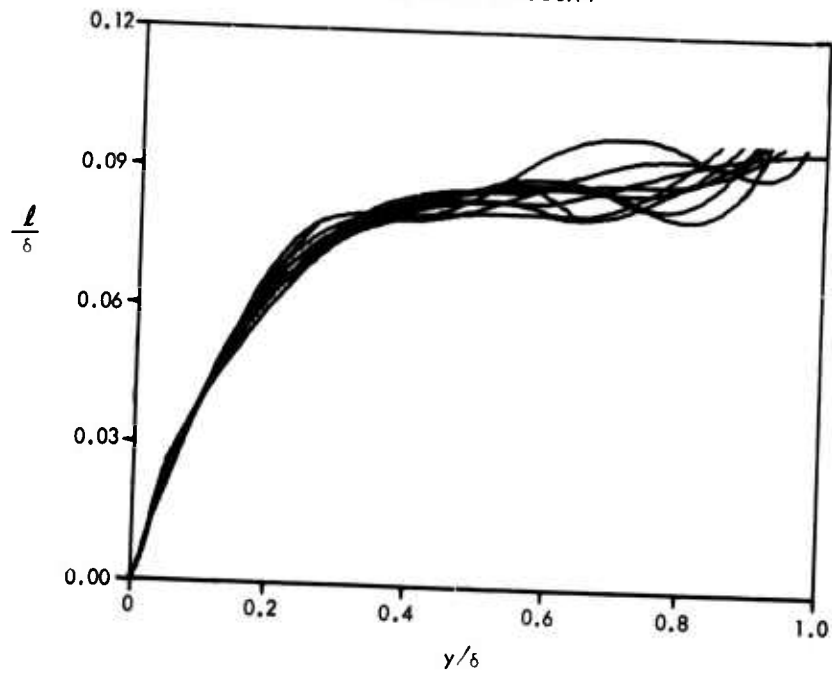


(b) SHEAR STRESS

FIG. 3-11 CALCULATED DISTRIBUTIONS FOR FLOW 1400,
WIEGHARDT-TILLMANN ZERO PRESSURE GRADIENT
FLOW ($\beta = 0$)



(c) EDDY VISCOSITY



(d) MIXING LENGTH

FIG. 3-11 (CONTINUED)

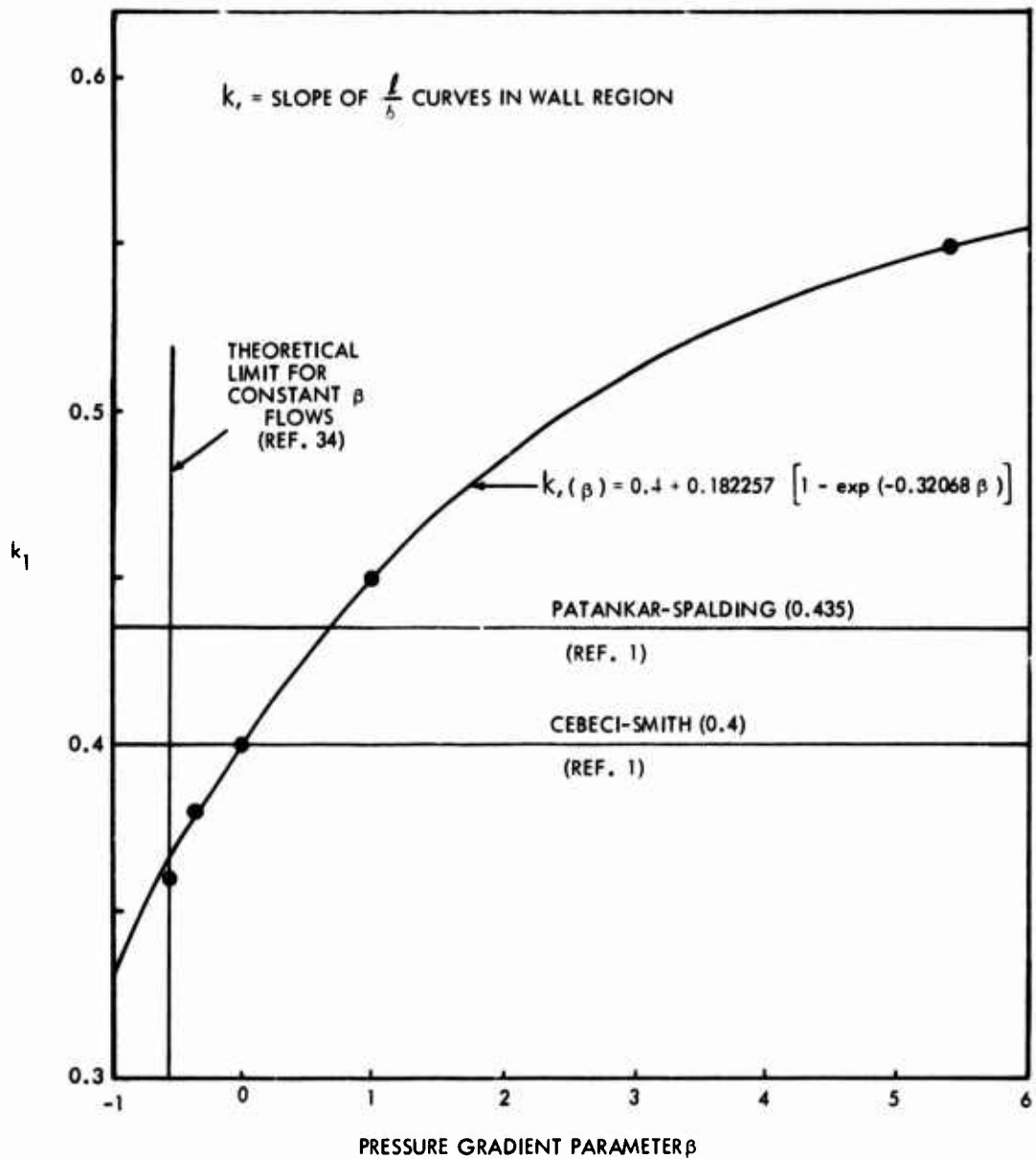


FIG. 3-12 VARIATION OF INNER MIXING LENGTH CONSTANT WITH PRESSURE GRADIENT PARAMETER β FOR EQUILIBRIUM FLOWS

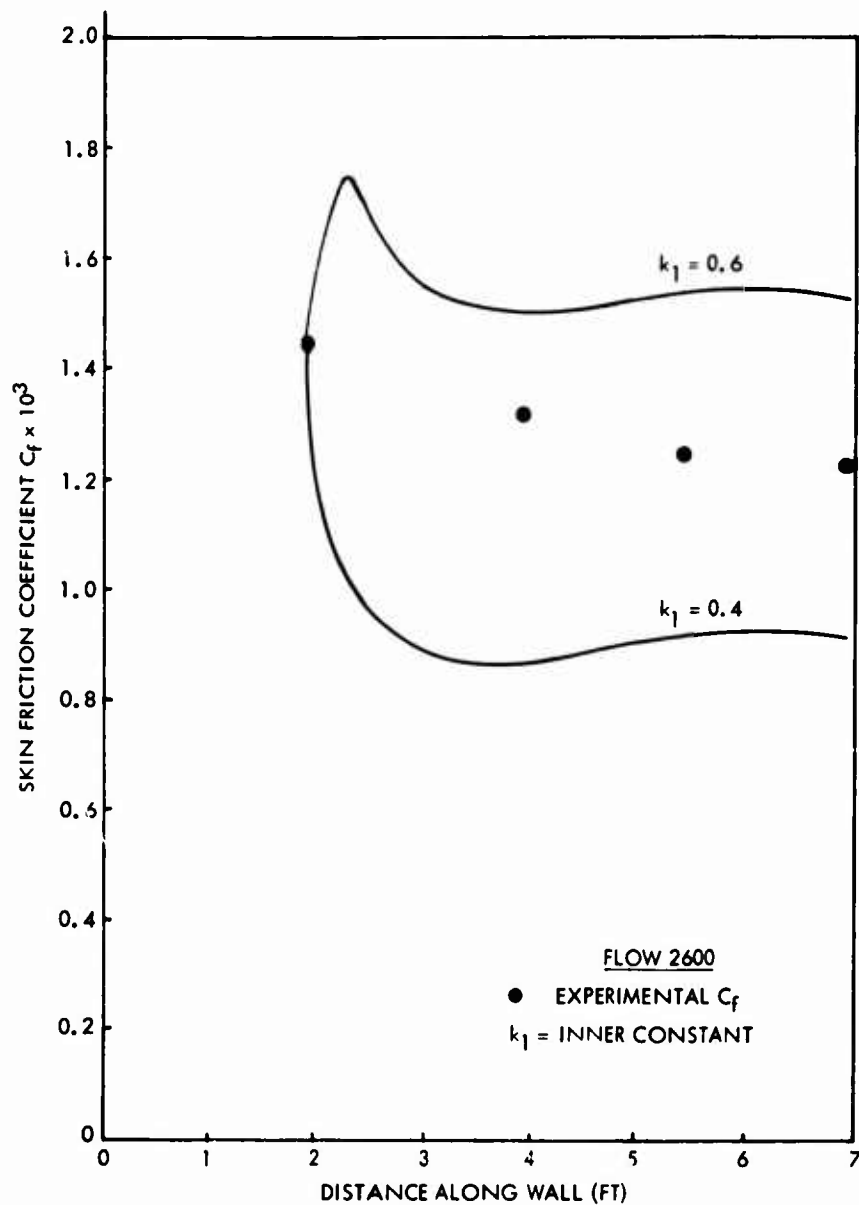


FIG. 4-1 EFFECT OF INNER MIXING LENGTH CONSTANT ON CALCULATED SKIN FRICTION DISTRIBUTION USING CEBECI-SMITH PROCEDURE AND EDDY VISCOSITY MODEL

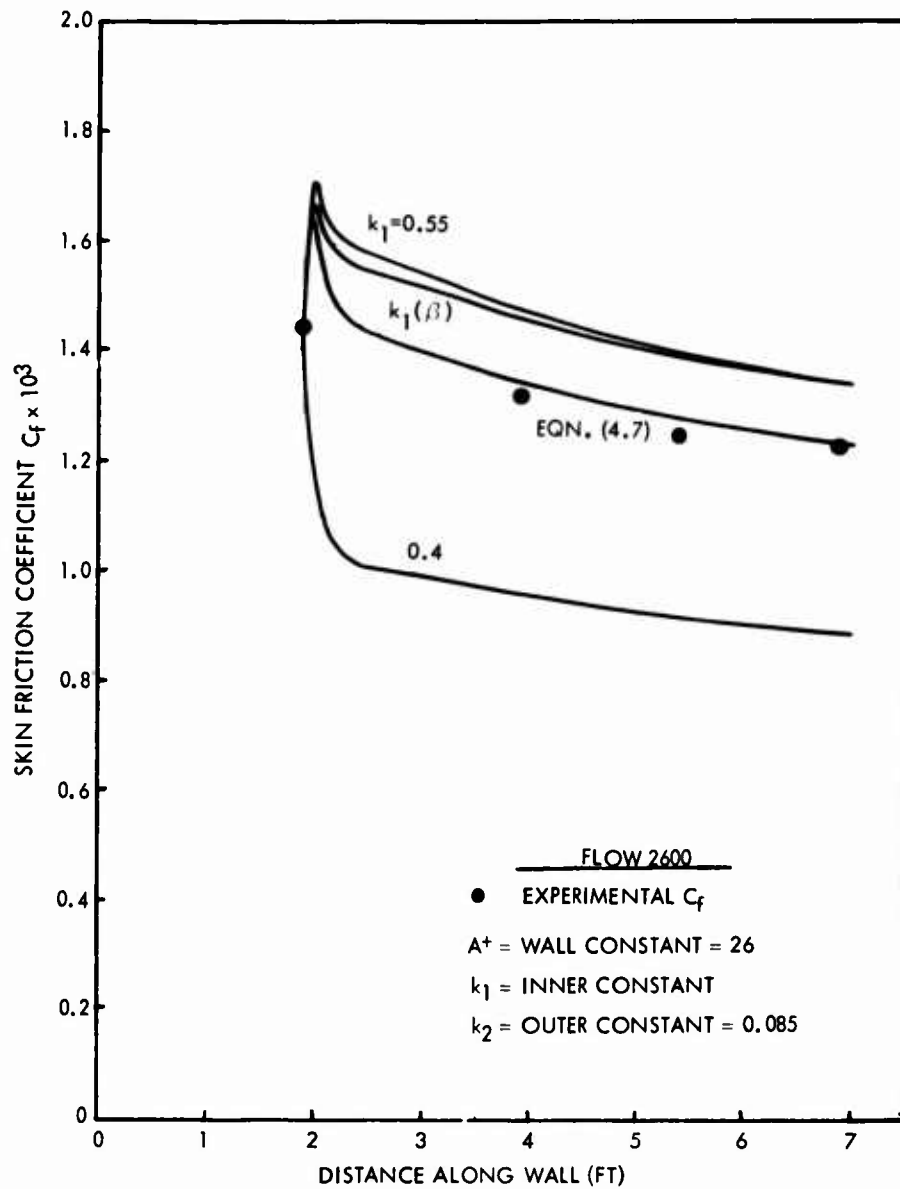


FIG. 4-2 EFFECT OF INNER MIXING LENGTH CONSTANT ON CALCULATED SKIN FRICTION DISTRIBUTION USING CEBECI-SMITH PROCEDURE

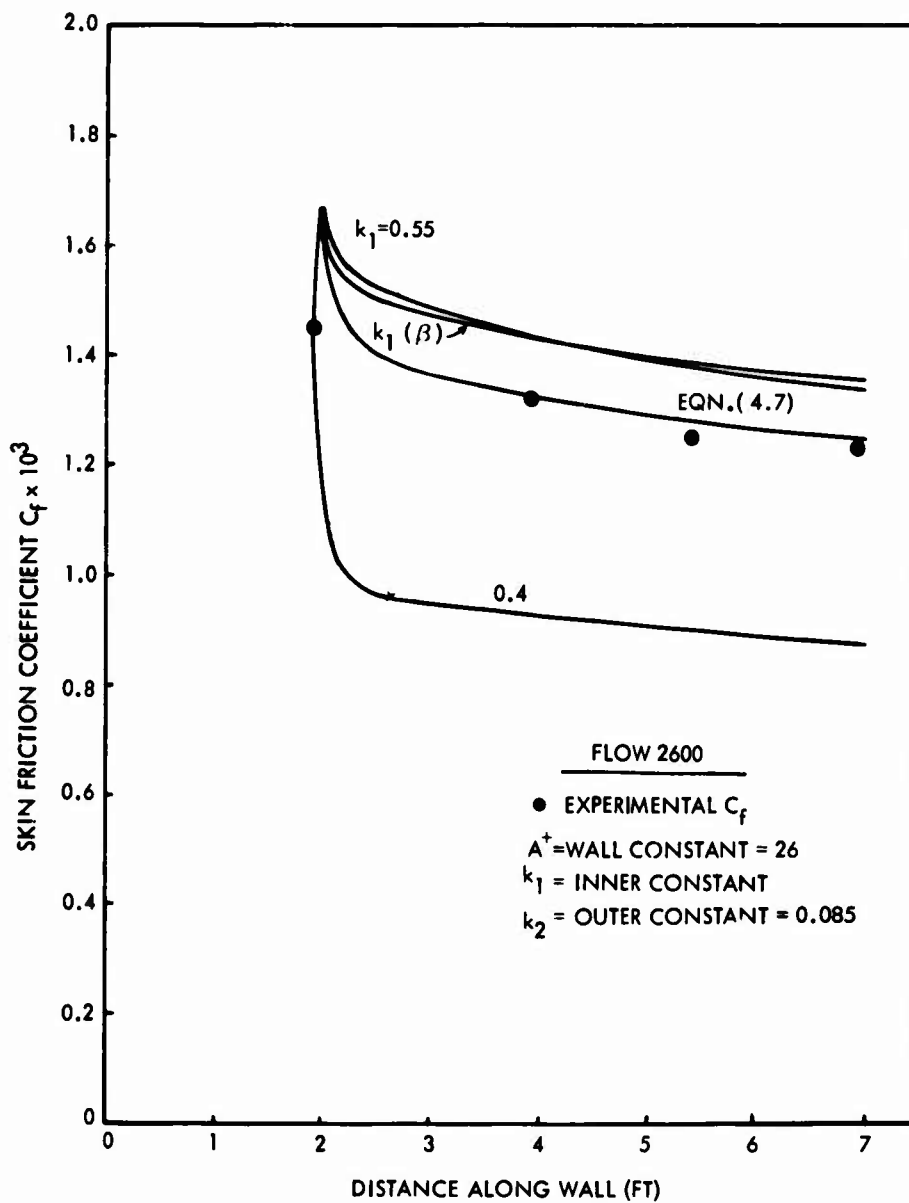


FIG. 4-3 EFFECT OF INNER MIXING LENGTH CONSTANT ON CALCULATED SKIN FRICTION DISTRIBUTION USING PRESENT PROCEDURE

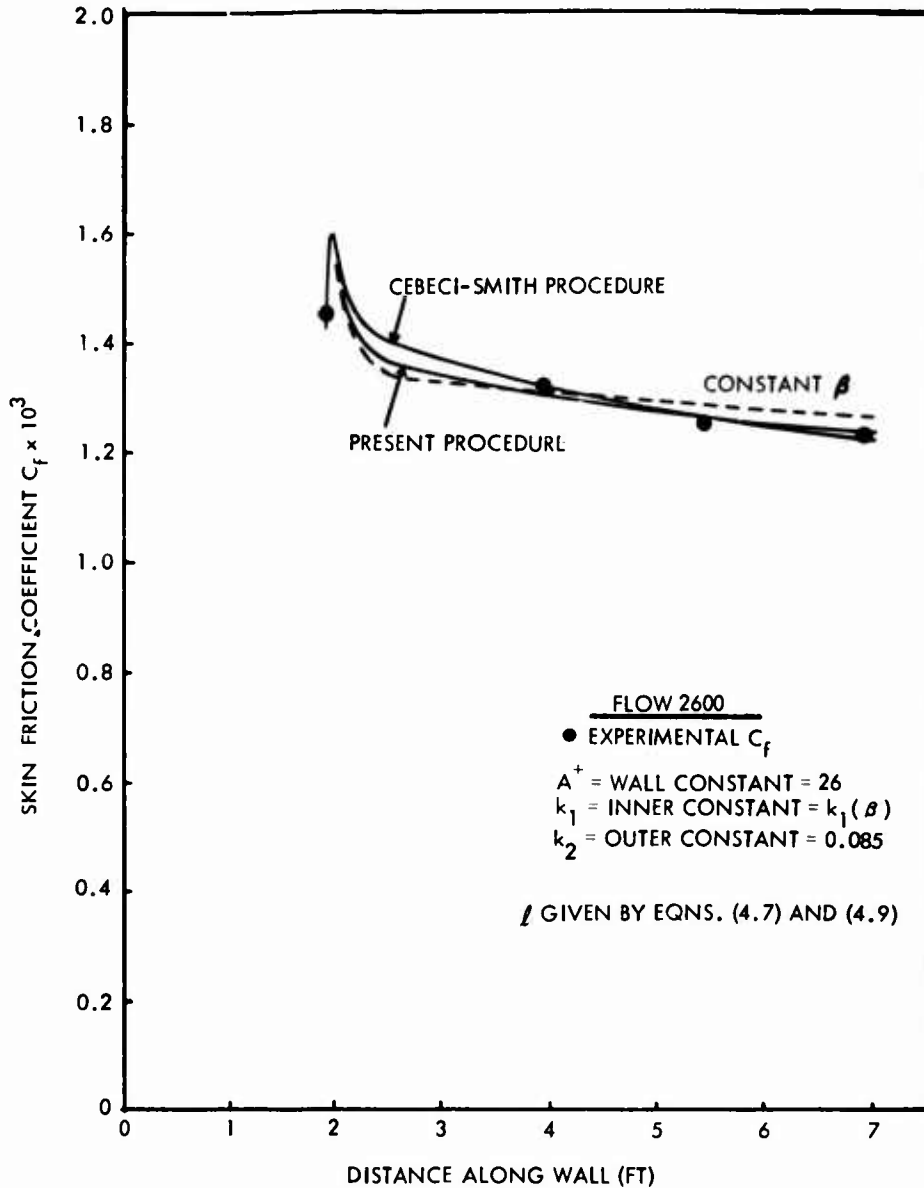
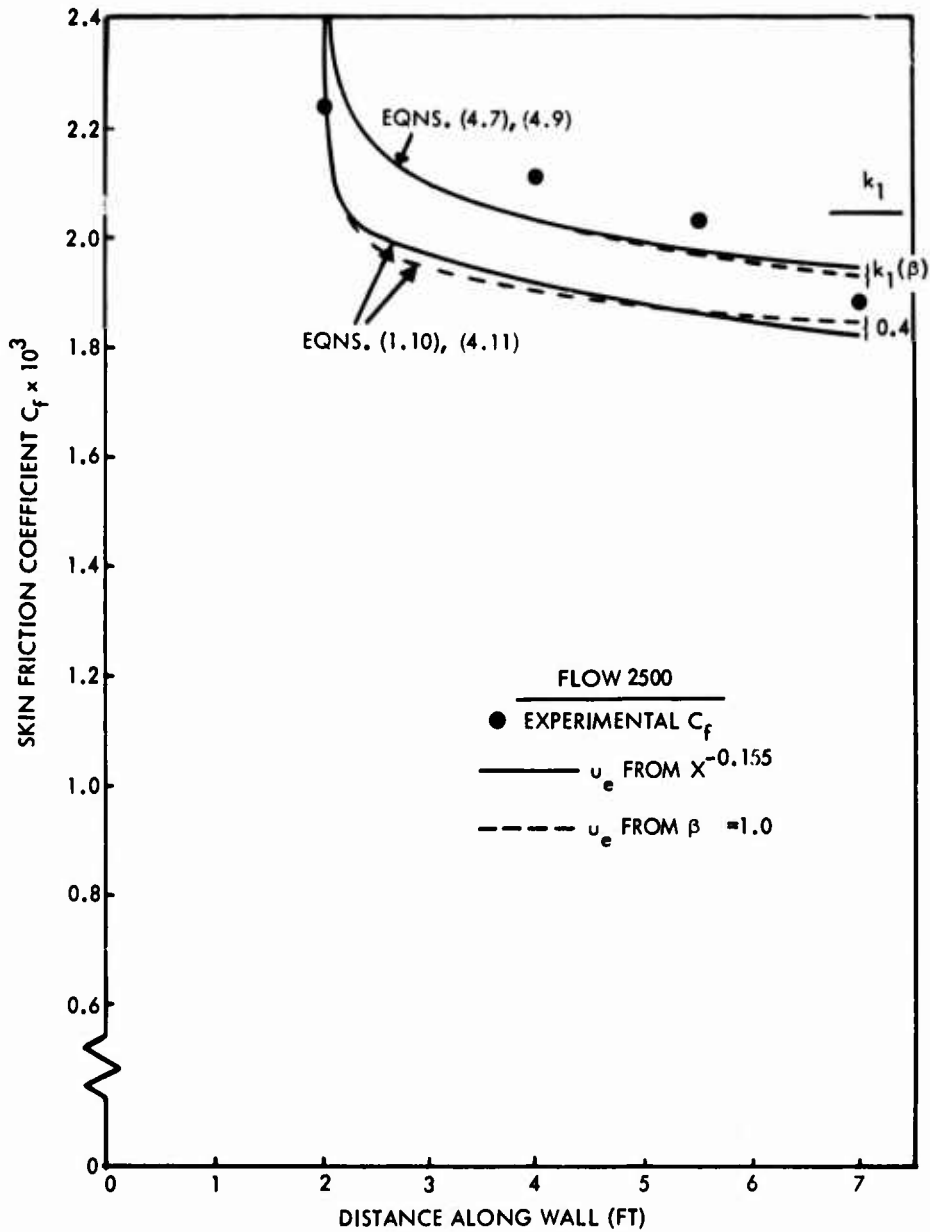


FIG. 4-4 SKIN FRICTION DISTRIBUTIONS CALCULATED WITH SUGGESTED MIXING LENGTH FORMULA USING VARIOUS PROCEDURES - FLOW 2600, BRADSHAW-FERRISS EQUILIBRIUM FLOW ($\beta \approx 5$)



(4.9)

FIG. 4-5 SKIN FRICTION DISTRIBUTIONS CALCULATED WITH VARIOUS MIXING LENGTH FORMULAS - FLOW 2500, BRADSHAW EQUILIBRIUM FLOW ($\beta \approx 1$)